R. & M. No. 3375

MINISTRY OF AVIATION

AERONAUTICAL RESEARCH COUNCIL
REPORTS AND MEMORANDA

Non-Linear Theory of Steady Forces on Wings with Leading-Edge Flow Separation

By H. C. GARNER, M.A., A.F.R.Ae.S. and
DORIS E. LEHRIAN, B.Sc.

LONDON: HER MAJESTY'S STATIONERY OFFICE
1964
PRICE £1 6s. 0d. NET

Non-Linear Theory of Steady Forces on Wings with Leading-Edge Flow Separation

By H. C. GARNER, M.A., A.F.R.Ae.S. and
DORIS E. LEHRIAN, B.Sc.

*Reports and Memoranda No. 3375**
February, 1963

Summary.

Leading-edge separation from fairly thin wings of moderate or low aspect ratio gives rise to aerodynamic loading and forces that are non-linear with incidence. It is important to be able to estimate these effects theoretically for wings of arbitrary planform. A simplified mathematical vortex model has been devised by Gersten for wings in steady incompressible flow. This model in conjunction with Multhopp's linear lifting-surface theory provides the basis of the present method.

The investigation covers a variety of planforms, and each type serves to illustrate different facets of non-linear theory and its numerical application. Many comparisons between the calculated results and wind-tunnel measurements are used in a critical appraisal of the method. When there are leading-edge vortices or extensive regions of separated flow, the calculated total lift and pitching moment give a decisive improvement on linear theory. Analysis shows a simple correlation between the centre of non-linear lift and the linear aerodynamic centre. The spanwise distributions of lift and local centre of pressure on rectangular wings are well predicted, but the calculated loading on swept wings appears to be unrealistic.

An alternative treatment of the mathematical model on the basis of slender-wing theory illustrates some defects of the method in its present form. It might be developed to simulate the rolling-up of vortex sheets into concentrated vortices. However, the reliability of the present method for steady aerodynamic forces appears to justify its immediate extension to the oscillatory problem of slowly pitching wings of arbitrary planform at high mean incidence.

LIST OF CONTENTS

* Replaces N.P.L. Aero Report No. 1059—A.R.C. 24 523. Published with the permission of the Director, National Physical Laboratory.

LIST OF TABLES

LIST OF ILLUSTRATIONS

1. *Introduction.*

Conventional aircraft of past decades were designed to fly without extensive regions of separated flow from the wing surface. Leading-edge separation without immediate reattachment was synonymous with stalling. Nowadays wings have greater sweepback and lower aspect ratio and commonly develop leading-edge vortices before the maximum usable lift coefficient is reached, but the associated increase in lift is rather small. The trend in planform continues in studies for supersonic aircraft, which envisage wings of increasing slenderness with sharp leading edges. Such aircraft are likely to have flow separation from the leading edge over most of their flight path. Moreover, during take-off and landing, up to one third of the lift may be associated directly with non-linear effects of flow separation. The estimation of these effects has now become an essential feature of aircraft design.

Theories are required to estimate the wing loading as a non-linear function of incidence. One basic concept is that, when vorticity is shed forward of the trailing edge, this vorticity is displaced from the wing so as to diminish its contribution to the downwash at the surface; in consequence extra vorticity or lift is required to maintain tangential flow there. This concept only applies when a mathematical model of the flow is appropriate. One of the earliest attempts on such lines was the work of Bollay[1] (1939) for rectangular wings of small aspect ratio. Several authors have since developed mathematical models for delta wings with varying degrees of success. More recently Gersten[2] (1961) has published a non-linear theory that in principle is applicable to any planform in steady incompressible flow; the theory uses the linear equations of motion, but introduces terms involving the square of the incidence. Gersten[3] (1961) has also reviewed the theoretical background to his work, and in both Refs. 2 and 3 experimental results are given to support his theory and justify its simplicity.

The present work envisages an extension of the theory to the problem of unsteady flow past slowly pitching wings about a high mean incidence. Whereas Gersten associates his theory with the linear lifting-surface theory of Truckenbrodt[4] (1953), our extension of the theory requires the substitution of Multhopp's[5] (1950) linear theory in place of Ref. 4. During the course of the work it has become apparent that a critical appraisal of the steady theory should precede the publication of the unsteady theory (Ref. 6).

After a general description of Gersten's theory (Section 2), its formal combination with Multhopp's theory is set out (Section 3). Considerable difficulties have arisen in specifying a numerical procedure, and the scheme devised for non-rectangular wings in Section 4.2 differs significantly from that used by Gersten. The convergence of the theoretical results and comparisons with experiment are discussed in Sections 5 and 6, which clarify the imperfections and achievements of the theory.

From the numerical standpoint the combined method is criticised on two counts. The approximate treatment of the central root section in Multhopp's theory assumes greater importance in the present application and becomes a likely source of error. Perhaps more serious is a singularity in the non-linear part of the boundary condition at the tip section, that would lead to divergence if the number of solving stations were increased indefinitely. For wings of very low aspect ratio both these criticisms can be avoided, if linear slender-wing theory is used and an approximation in Gersten's theory is removed (Section 7). There remains, however, a further criticism, that Gersten's mathematical model precludes the rolling-up of vortex sheets. When this occurs near the leading edge, as it usually does in the case of swept wings, the calculated load distributions are unrealistic.

Nevertheless the present method gives reliable predictions of overall steady forces in incompressible flow, and it is worthy of further development (Section 8).

2. *Gersten's Theory.*

2.1. *Mathematical Model.*

One of the earliest theoretical methods for determining non-linear effects of incidence is that developed by Bollay[1] (1939) for rectangular wings. The mathematical model, adopted by Bollay, has a continuous distribution of vortices trailing from the wing tips along straight lines inclined at an arbitrary, but constant, angle to the wing surface; this implies a uniform spanwise loading and flow separation at the wing tips. Bollay assumes that the aspect ratio is small, and he determines the strength and inclination of the vortices from average conditions that the flow is tangential along the centre-line and that the trailing vortices follow the streamlines initially. It can be seen from his iterative solutions in Fig. 13 of Ref. 1 that for very low aspect ratios the trailing vortices are inclined above the wing at an angle approximately equal to $\frac{1}{2}\alpha$; for finite aspect ratios ($A < 1$) the angle of inclination is 10 to 20% larger.

Gersten[2] has generalised Bollay's model by allowing the wing planform and its loading to be quite arbitrary, and he specifies that the trailing vorticity is shed from each point of the lifting surface at an angle of exactly $\frac{1}{2}\alpha$ to the plane of the wing. If we regard the wing as consisting of infinitesimal lifting elements, then Gersten has in effect applied Bollay's mathematical model to each lifting element. The condition of tangential flow is to be satisfied, but the streamline vortex condition is relaxed. A simple representation of Gersten's mathematical model is shown in Fig. 1a. The wing is without thickness and at a positive incidence α. All the vorticity is shed instantly in planar sheets above the wing inclined at an angle $\frac{1}{2}\alpha$ to the surface. Thus rotational flow occurs throughout a wake of finite constant cross-section, illustrated for various planforms in Fig. 1b. Nevertheless the flow at the wing can be built up as a superposition of elementary potential flows corresponding to planar vortex sheets. In reality flow separation involves singularities along separation lines in the wing surface, where free vortices originate. In the mathematical model it is supposed without physical justification, that the free vortices are shed at all points of the upper surface; moreover, there is a discontinuity of $\frac{1}{2}\alpha$ between the tangential surface flow and the direction in which the vorticity is assumed to be convected. Whilst the initial choice of angle $\frac{1}{2}\alpha$ is suggested by the results of Bollay's low-aspect-ratio theory, there is no flow condition that can be applied as an independent check on the angle.

The development of Gersten's theory is such that an arbitrary angle could be inserted to replace $\frac{1}{2}\alpha$ as a final step in the solution. There are reasons for supposing that the angle will be a decreasing function of Mach number. But for incompressible flow the value $\frac{1}{2}\alpha$ can be justified empirically by the comparisons between measured and calculated lift (Section 6). It should be noted that to the first order in α the mathematical model reduces to a vortex arrangement in the plane of the wing in accord with linear lifting-surface theory.

2.2. *Upwash Field from Linear Theory.*

The equations of linear theory can be formulated under the following assumptions. The wing is of negligible thickness, but may have small arbitrary incidence, camber and twist whose squares can be ignored: the free stream is inviscid, incompressible and of uniform velocity U: the squares and products of the non-dimensional velocity perturbations u/U, v/U and w/U are negligible: the flow is irrotational outside the vortex sheet formed by the wing and wake. With these assumptions the vortex sheet can be considered in a plane $z = 0$, and its strength can be determined from the boundary condition that the upward induced velocity

$$w(x, y, 0) = -U\alpha(x, y) = U\frac{\partial z(x, y)}{\partial x}, \tag{1}$$

where $z = z(x, y)$ is the equation of the wing surface and x is measured in the direction of the free stream.

Let $\Gamma(x', y')$ be the strength of the vortex sheet which, under the linear assumptions, corresponds to a lift per unit area

$$\Delta p = \tfrac{1}{2}\rho U^2 l(x', y') = \rho U\Gamma(x', y'). \tag{2}$$

It can be seen from equations (4), (10) and (12) of Ref. 5, that the upwash field is

$$w(x, y, z) = \frac{1}{4\pi}\int\int \Gamma(x', y')K(x-x', y-y', z)dx'\, dy', \tag{3}$$

where

$$\begin{aligned} K &= \int_{-\infty}^{x} \frac{\partial}{\partial z}\left(-\frac{z}{r^3}\right) dx \text{ with } r^2 = (x-x')^2 + (y-y')^2 + z^2 \\ &= \frac{(y-y')^2 - z^2}{[(y-y')^2 + z^2]^2}\left(1 + \frac{x-x'}{r}\right) - \frac{z^2}{(y-y')^2 + z^2}\left(\frac{x-x'}{r^3}\right). \end{aligned} \tag{4}$$

In the plane of the vortex sheet equations (3) and (4) become

$$w(x, y, 0) = w_0(x, y) = \frac{1}{4\pi}\int\int \frac{\Gamma(x', y')}{(y-y')^2}\left[1 + \frac{x-x'}{\{(x-x')^2 + (y-y')^2\}^{1/2}}\right] dx'\, dy', \tag{5}$$

where the principal value of the integral through $y' = y$ is defined in Appendix I of Ref. 5. From equations (3) and (4) the upwash $w(x, y, z)$ is clearly an even function of z. Superficially it may appear that w can be expanded in even powers of z, but there is in fact a term in $|z|$. This follows from equation (A5) of Appendix A, which will be seen to form the basis of Gersten's theory.

2.3. *Basic Equations.*

Equations (1), (2) and (5) combine to give the integral equation of linear theory, from which the non-dimensional wing loading $l(x', y')$ is determined as a linear function of the incidence. These equations are not very restrictive in α, since linear theory can be a good approximation in cases of unseparated flow at fairly high incidence. Gersten's theory is only non-linear in a restricted sense. In so far as they would affect equation (2), squares of u/U, v/U and w/U are still neglected. When Gersten's mathematical model applies, the upwash field will involve terms in α^2, while those in α^3 are neglected.

As shown in Fig. 1a, the rectangular axes Ox, y, z are referred to an origin of co-ordinates at the leading edge of the centre-line. It is convenient to take the z-axis normal to the elementary vortex sheets, so that they lie in parallel planes $z = z'$ and the wing lies in the plane

$$z = -\tfrac{1}{2}\alpha x. \tag{6}$$

If $\Gamma(x, y)$ denotes the strength of a vortex sheet in the plane $z = z'$, then the neighbouring upwash field from equation (A5) of Appendix A is

$$w(x, y, z) = w_0 - \tfrac{1}{2}\,|\,z - z'\,|\,\left\{\frac{\partial\Gamma}{\partial x} + \frac{\partial^2}{\partial y^2}\left[\int_{-\infty}^{x} \Gamma(x_0, y)dx_0\right]\right\} + O(z-z')^2, \tag{7}$$

provided that $\Gamma(x_0, y)$ is a sufficiently well-behaved function. The elementary potential flows correspond to a bound vortex of strength $\tfrac{1}{2}Ul(x', y)\delta x'$ at $x = x'$ and the associated trailing vorticity in the plane $z = z' = -\tfrac{1}{2}\alpha x'$. Thus the elementary vortex sheet is defined by

$$\left.\begin{aligned} \Gamma(x, y) &= 0 & x < x' \\ \int_{-\infty}^{x} \Gamma(x_0, y)dx_0 &= \tfrac{1}{2}Ul(x', y)\delta x' & x > x' \end{aligned}\right\}. \tag{8}$$

Since $\partial\Gamma/\partial x = 0$ for $x > x'$, equations (7) and (8) combine to give an elementary contribution

$$\delta w(x, y, z) = \delta w_0 - \tfrac{1}{2}|z - z'|\,\frac{\partial^2}{\partial y^2}\,[\tfrac{1}{2}Ul(x', y)]\delta x', \text{ when } x' < x;$$

as explained at the end of Appendix A,

$$\delta w(x, y, z) = \delta w_0, \text{ when } x' > x \text{ outside the range of integration.}$$

Integration with respect to x' gives

$$w(x, y, z) = w_0(x, y) - \frac{U}{4}\int_{-\infty}^{x} |z - z'|\,\frac{\partial^2}{\partial y^2}\,[l(x', y)]dx', \tag{9}$$

where $z' = -\tfrac{1}{2}\alpha x'$ and on the wing surface $z = -\tfrac{1}{2}\alpha x$. Thus by equations (5) and (9)

$$\begin{aligned} w(x, y, -\tfrac{1}{2}\alpha x) = {} & \frac{U}{8\pi}\iint\limits_{S} \frac{l(x', y')}{(y-y')^2}\left[1 + \frac{x - x'}{\{(x-x')^2 + (y-y')^2\}^{1/2}}\right] dx'dy' - \\ & - \frac{U\alpha}{8}\,\frac{\partial^2}{\partial y^2}\left[\int_{x_l}^{x} l(x', y)\,(x-x')dx'\right], \end{aligned} \tag{10}$$

where S denotes integration over the wing planform and $x = x_l(y)$ is the equation of the leading edge.

Referred to the axes of Fig. 1a the free-stream velocity is

$$(U \cos \tfrac{1}{2}\alpha,\, 0,\, U \sin \tfrac{1}{2}\alpha) = (U, 0, \tfrac{1}{2}U\alpha).$$

By equation (6) $(\tfrac{1}{2}\alpha, 0, 1)$ represents a normal to the wing surface. The local velocity $(U+u, v, \tfrac{1}{2}U\alpha+w)$ is tangential to the wing, if

$$w + \tfrac{1}{2}u\alpha = -U\alpha. \tag{11}$$

The term $\tfrac{1}{2}u\alpha$ in equation (11) may be neglected, since the element (8) contributes

$$\begin{aligned} \delta u &= (\delta u)_{z=z'} + (z-z')\,\frac{\partial}{\partial z}(\delta u) + O(z-z')^2 \\ &= 0 + (z-z')\,\frac{\partial}{\partial x}(\delta w) + O(z-z')^2 \\ &= O(\alpha^2). \end{aligned}$$

Therefore the boundary condition to replace equation (1) is

$$w(x, y, -\tfrac{1}{2}\alpha x) = -U\alpha = U\frac{\partial z}{\partial x} - \tfrac{1}{2}U\alpha. \tag{12}$$

The term $U\,\partial z/\partial x$ may include linear terms in camber and twist, just as they would occur in equation (1); but Gersten's mathematical model implies that their products with incidence are negligible.

The final integral equations are obtained from equations (10) and (12) by writing

$$l(x', y') = \alpha l_1(x', y') + \alpha^2 l_{11}(x', y') \tag{13}$$

and equating the terms in α and α^2. By equation (13) the lift and pitching moment become quadratic functions of α.

It is stressed that the approximation in equation (7) is distinct from that associated with Gersten's mathematical model. Both approximations are necessary in order to achieve a tractable method for a wing of arbitrary planform. At first sight equation (10) suggests that, since $w/U = O(\alpha)$ and the last term is $O(\alpha^2)$, terms in $(w/U)^2$ cannot be neglected consistently elsewhere in the analysis. There is, however, some justification, when the aspect ratio A is not large; then the last term of equation (10) becomes appreciable at fairly low incidences, well within the accepted range for the linear theory of unseparated flow. We may regard this term as $O(\alpha^2/A)$ and quite distinct from smaller terms of order $(w/U)^2$ that arise independently.

3. *Formulation of Present Method.*

From the account of Gersten's non-linear theory in Section 2 it is clear that any linear theory can be used as a starting point. The present method results when Multhopp's[5] lifting-surface theory provides the linear basis.

3.1. *Multhopp's Linear Theory.*

The linear boundary condition from equations (1), (2) and (5) is

$$\alpha(x, y) = -\frac{w}{U} = -\frac{1}{8\pi}\iint\limits_S \frac{l(x', y')}{(y-y')^2}\left[1 + \frac{x - x'}{\{(x-x')^2 + (y-y')^2\}^{1/2}}\right] dx'dy', \tag{14}$$

which corresponds to equation (15) of Ref. 5. At each section y' the chordwise loading is expressed as $N(\leqslant 4)$ terms of a series

$$\begin{aligned} l(x', y') = \frac{8s}{\pi c(y')}\,[\gamma(y') \cot \tfrac{1}{2}\phi' &+ 4\mu(y')\,(\cot \tfrac{1}{2}\phi' - 2\sin\phi') + \\ &+ \kappa(y')\,(\cot\tfrac{1}{2}\phi' - 2\sin\phi' - 2\sin 2\phi') + \\ &+ \lambda(y')\,(\cot\tfrac{1}{2}\phi' - 2\sin\phi' - 2\sin 2\phi' - 2\sin 3\phi')]\,. \end{aligned} \tag{15}$$

Here s is the semi-span of the wing, and

$$x' = x_l(y') + \tfrac{1}{2}c(y')\,(1 - \cos\phi'), \tag{16}$$

where $c(y')$ is the local chord and $x_l(y')$ is the ordinate of the leading edge.

The chordwise integration of equation (14) gives

$$\alpha(x, y) = -\frac{s}{2\pi}\int_{-s}^{s} \frac{\gamma i + \mu j + \kappa k + \lambda l}{(y-y')^2}\, dy', \tag{17}$$

introducing influence functions $i(X, Y)$, $j(X, Y)$, $k(X, Y)$ and $l(X, Y)$; for example,

$$k(X, Y) = \frac{1}{\pi}\int_0^\pi (\cot\tfrac{1}{2}\phi' - 2\sin\phi' - 2\sin 2\phi')\left[1 + \frac{X - \frac{1}{2}(1-\cos\phi')}{[\{X - \frac{1}{2}(1-\cos\phi')\}^2 + Y^2]^{1/2}}\right]\sin\phi'\,d\phi', \qquad (18)$$

where

$$\left.\begin{aligned} X &= \{x - x_l(y')\}/c(y') \\ Y &= (y-y')/c(y') \end{aligned}\right\}.$$

Multhopp's original work is restricted to $N = 2$. It may be noted that, if $N = 3$ (i.e. $\lambda = 0$), then all three influence functions can be evaluated from Ref. 7; i and j are tabulated explicitly, and the formula

$$k = 2i - \tfrac{1}{4}j - 2jj$$

gives k in terms of these and jj which is also tabulated in Ref. 7. In practice, a mechanized programme is used to compute the influence functions.

The spanwise integration of equation (17) is achieved by Multhopp's technique of interpolation in which the functions γ, μ, κ, λ are represented by polynomials in terms of their values at the m collocation stations

$$y' = s\eta_n = s\sin\frac{\pi n}{m+1}\ [n = 0, \pm 1, \pm 2, \ldots \pm\tfrac{1}{2}(m-1)],$$

where m is an odd integer. Thus

$$\alpha(x, y_\nu) = \alpha_\nu(x) = b_{\nu\nu}(\gamma\bar{i} + \mu\bar{j} + \kappa\bar{k} + \lambda\bar{l})_\nu - \sum_{-(m-1)/2}^{(m-1)/2}{}' b_{\nu n}(\gamma i + \mu j + \kappa k + \lambda l)_n, \qquad (19)$$

where

$$\left.\begin{aligned} b_{\nu\nu} &= \frac{m+1}{4\sqrt{(1-\eta_\nu^2)}} \\ b_{\nu n} &= \frac{\sqrt{(1-\eta_n^2)}}{(m+1)\,(\eta_n - \eta_\nu)^2} \quad |\nu - n| = 1, 3, 5, \ldots \\ &= 0 \qquad\qquad\qquad\qquad |\nu - n| = 2, 4, 6, \ldots \end{aligned}\right\}, \qquad (20)$$

the suffix ν denotes that $y = s\eta_\nu = s\sin\{\nu\pi/(m+1)\}$ $[\nu = 0, \pm 1, \pm 2, \ldots \pm\frac{1}{2}(m-1)]$, and Σ' denotes that the value $n = \nu$ is not included in the summation. There are logarithmic singularities in the derivatives of i, j, k and l with respect to Y, which contribute to the first term of equation (19); following Mangler and Spencer[8] we obtain

$$(\gamma\bar{i} + \mu\bar{j} + \kappa\bar{k} + \lambda\bar{l})_\nu = \gamma_\nu\bar{i}_\nu + \mu_\nu\bar{j}_\nu + \kappa_\nu\bar{k}_\nu + \lambda_\nu\bar{l}_\nu,$$

where

$$\left.\begin{aligned} \bar{i}_\nu &= \frac{2}{\pi}(\phi + \sin\phi) + \left(\frac{s}{c_\nu}\right)^2 \frac{4G_\nu}{\pi\sin\phi(1-\cos\phi)} \\ \tfrac{1}{4}\bar{j}_\nu &= \frac{2}{\pi}(\sin\phi + \tfrac{1}{2}\sin 2\phi) + \left(\frac{s}{c_\nu}\right)^2 \frac{4G_\nu(2\cos\phi - \cos 2\phi)}{\pi\sin\phi(1-\cos\phi)} \\ \bar{k}_\nu &= \frac{2}{\pi}(\tfrac{1}{2}\sin 2\phi + \tfrac{1}{3}\sin 3\phi) + \left(\frac{s}{c_\nu}\right)^2 \frac{4G_\nu(3\cos 2\phi - 2\cos 3\phi)}{\pi\sin\phi(1-\cos\phi)} \\ \bar{l}_\nu &= \frac{2}{\pi}(\tfrac{1}{3}\sin 3\phi + \tfrac{1}{4}\sin 4\phi) + \left(\frac{s}{c_\nu}\right)^2 \frac{4G_\nu(4\cos 3\phi - 3\cos 4\phi)}{\pi\sin\phi(1-\cos\phi)} \\ G_\nu &= \frac{1}{m+1}(\log_e 2 + \tfrac{1}{2} - \eta_\nu^2) + \frac{4}{(m+1)^2}\sum_{-(m-1)/2}^{(m-1)/2}{}'(1-\eta_n^2)\log_e|\eta_\nu - \eta_n| \\ x &= (x_l)_\nu + \tfrac{1}{2}c_\nu(1-\cos\phi) \end{aligned}\right\}. \qquad (21)$$

At the kinked central section of a swept wing, Multhopp evaluates equation (19) for an 'interpolated wing' (Ref. 5, Section 5.3), such that $x_l(0) = 0$ and $c(0) = c_r$ are replaced respectively by

$$\left.\begin{aligned} (x_l)_0 &= \frac{1}{6}(x_l)_1 \\ c_0 &= \frac{5}{6}c_r + \frac{1}{6}c_1 \end{aligned}\right\} \tag{22}$$

in terms of the neighbouring collocation station $n = 1$.

With the aid of equations (18) to (22), equation (19) can be evaluated for arbitrary x. By choosing

$$\phi_p = \frac{2p\pi}{2N+1}\,(p = 1, 2, \ldots N) \tag{23}$$

and hence

$$x = x_{p\nu} = (x_l)_\nu + \tfrac{1}{2}c_\nu(1-\cos\phi_p), \tag{24}$$

and specifying the values of $\alpha(x_{p\nu}, y_\nu)$ for the mN pairs of values (p, ν), we derive the linear solution by collocation from a set of linear simultaneous equations for the mN variables γ_n, μ_n, etc. The local lift coefficient at $\eta = \eta_n$ and centre of pressure measured as a fraction of the local chord from the leading edge are respectively

$$C_{LL} = \frac{4s\gamma_n}{c_n} \tag{25}$$

and

$$\left.\begin{aligned} X_{cp} &= \frac{1}{4} - \frac{\mu_n}{\gamma_n}\,(n \neq 0) \\ (X_{cp})_0 &= \frac{1}{c_r}\left\{\frac{1}{6}(x_l)_1 + c_0\left(\frac{1}{4} - \frac{\mu_0}{\gamma_0}\right)\right\} \end{aligned}\right\}. \tag{26}$$

The total lift coefficient is

$$\begin{aligned} C_L &= \frac{1}{2}\int_{-1}^{1} C_{LL}\frac{c}{\bar{c}}\,d\eta = A\int_{-1}^{1}\gamma\,d\eta \\ &= \frac{\pi A}{m+1}\sum_{-(m-1)/2}^{(m-1)/2}\gamma_n\sqrt{(1-\eta_n^2)}. \end{aligned} \tag{27}$$

The total pitching-moment coefficient about an axis $x = x_0$ is

$$\begin{aligned} C_m &= \frac{A}{\bar{\bar{c}}}\int_{-1}^{1}\gamma(x_0 - x_l - X_{cp}c)\,d\eta \\ &= \frac{\pi A}{\bar{\bar{c}}(m+1)}\sum_{-(m-1)/2}^{(m-1)/2}\left[\mu_n c_n + \gamma_n\{x_0 - (x_l)_n - \tfrac{1}{4}c_n\}\right]\sqrt{(1-\eta_n^2)}, \end{aligned} \tag{28}$$

where the aerodynamic mean chord

$$\bar{\bar{c}} = \int_0^1 c^2\,d\eta \bigg/ \int_0^1 c\,d\eta \tag{29}$$

and the aerodynamic quarter-chord axis corresponds to

$$\left.\begin{aligned} x_0 &= \int_0^1 (x_l + \tfrac{1}{4}c)c\,d\eta \bigg/ \int_0^1 c\,d\eta \\ &= \bar{\bar{x}}_l + \tfrac{1}{4}\bar{\bar{c}} \end{aligned}\right\}. \tag{30}$$

Hence

$$C_m = \frac{\pi A}{(m+1)} \sum_{-(m-1)/2}^{(m-1)/2} \left[\mu_n \frac{c_n}{\bar{\bar{c}}} + \gamma_n \left\{\frac{\bar{\bar{x}}_l - (x_l)_n}{\bar{c}} + \frac{\bar{c} - c_n}{4\bar{c}}\right\}\right] \sqrt{(1-\eta_n^2)}\,. \quad (31)$$

3.2. *Non-Linear Theory.*

In the notation of Section 2 the load distribution is expressed as

$$l = l_1\alpha + l_{11}\alpha^2, \quad (32)$$

where α is the positive uniform incidence of the wing. Then by equations (10) and (12), l_1 is precisely the linear solution from Section 3.1 with $\alpha(x, y) = \alpha_1 = 1$. The terms in α^2 in equation (10) lead to a similar integral for l_{11} which is identified with the linear solution for

$$\alpha(x, y) = \alpha_{11} = -\frac{1}{8}\frac{\partial^2}{\partial y^2}\left[\int_{x_l}^{x} l_1(x', y)\,(x-x')dx'\right], \quad (33)$$

where l_1 is given by equation (15) with $\gamma(y')$ replaced by $\gamma_1(y)$ and so on. Hence

$$\int_{x_l}^{x} l_1(x', y)\,(x-x')dx' = \frac{2sc(y)}{\pi}\,[\gamma_1(y)I_1(\phi) + \mu_1(y)J_1(\phi) + \kappa_1(y)K_1(\phi) + \lambda_1(y)L_1(\phi)]\,, \quad (34)$$

where

$$\left.\begin{aligned} I_1(\phi) &= \int_0^\phi (\cos\phi' - \cos\phi)\,(1+\cos\phi')d\phi' \\ J_1(\phi) &= 4\int_0^\phi (\cos\phi' - \cos\phi)\,(\cos\phi' + \cos 2\phi')d\phi' \\ K_1(\phi) &= \int_0^\phi (\cos\phi' - \cos\phi)\,(\cos 2\phi' + \cos 3\phi')d\phi' \\ L_1(\phi) &= \int_0^\phi (\cos\phi' - \cos\phi)\,(\cos 3\phi' + \cos 4\phi')d\phi' \end{aligned}\right\}. \quad (35)$$

Therefore

$$\alpha_{11} = -\frac{1}{2\pi A}\frac{\partial^2 f}{\partial \eta^2}, \quad (36)$$

where

$$f = \frac{c\gamma_1}{\bar{c}}\,I_1(\phi) + \frac{c\mu_1}{\bar{c}}\,J_1(\phi) + \frac{c\kappa_1}{\bar{c}}\,K_1(\phi) + \frac{c\lambda_1}{\bar{c}}\,L_1(\phi),$$

$c\gamma_1/\bar{c}$, $c\mu_1/\bar{c}$, . . . are specified by their values at the collocation stations $\eta = \eta_\nu = \sin\{\nu\pi/(m+1)\}$ and ϕ may also depend on η through the relationship

$$x = x_l(\eta) + \tfrac{1}{2}c(\eta)\,(1 - \cos\phi)\,. \quad (37)$$

The evaluation of $\alpha_{11}(x_{p\nu}, y_\nu)$ is considered in Section 4 and needs special care. The values at the mN collocation points are substituted in equation (19) to determine the numerical values of γ_{11}, μ_{11}, κ_{11} and λ_{11} and hence

$$\begin{aligned} l_{11}(x, \eta_n) = \frac{8s}{\pi c_n}\,[(\gamma_n)_{11}\cot\tfrac{1}{2}\phi &+ (\mu_n)_{11}(\cot\tfrac{1}{2}\phi - 2\sin\phi) + \\ &+ (\kappa_n)_{11}(\cot\tfrac{1}{2}\phi - 2\sin\phi - 2\sin 2\phi) + \\ &+ (\lambda_n)_{11}(\cot\tfrac{1}{2}\phi - 2\sin\phi - 2\sin 2\phi - 2\sin 3\phi)]\,. \quad (38) \end{aligned}$$

It remains to determine C_{LL}, X_{cp}, C_L and C_m by setting

$$\left.\begin{aligned} \gamma_n &= (\gamma_n)_1\alpha + (\gamma_n)_{11}\alpha^2 \\ \mu_n &= (\mu_n)_1\alpha + (\mu_n)_{11}\alpha^2 \end{aligned}\right\} \tag{39}$$

in the respective equations (25), (26), (27) and (31). The lift and pitching-moment coefficients are conveniently written as

$$\left.\begin{aligned} C_L &= a_1\alpha + a_{11}\alpha^2 \\ C_m &= m_1\alpha + m_{11}\alpha^2 \end{aligned}\right\}. \tag{40}$$

The spanwise lift distribution is obtained as

$$\frac{cC_{LL}}{\bar{c}C_L} = \frac{2(m+1)\,\{(\gamma_n)_1 + \alpha(\gamma_n)_{11}\}}{\pi \sum\limits_{-(m-1)/2}^{(m-1)/2} \{(\gamma_n)_1 + \alpha(\gamma_n)_{11}\}\,\sqrt{(1-\eta_n^2)}}, \tag{41}$$

and the local centre of pressure is

$$\left.\begin{aligned} X_{cp} &= \frac{1}{4} - \frac{(\mu_n)_1 + \alpha(\mu_n)_{11}}{(\gamma_n)_1 + \alpha(\gamma_n)_{11}}\ (n \neq 0) \\ (X_{cp})_0 &= \frac{1}{c_r}\left\{\frac{1}{6}(x_l)_1 + c_0\left(\frac{1}{4} - \frac{(\mu_0)_1 + \alpha(\mu_0)_{11}}{(\gamma_0)_1 + \alpha(\gamma_0)_{11}}\right)\right\} \end{aligned}\right\}. \tag{42}$$

4. *Methods of Calculation.*

4.1. *Rectangular Wings.*

In the particular case of a rectangular wing the evaluation of equation (36) presents little difficulty. We have

$$\alpha_{11} = -\frac{1}{2\pi A}\frac{\partial^2}{\partial\eta^2}[\gamma_1 I_1(\phi) + \mu_1 J_1(\phi) + \kappa_1 K_1(\phi) + \lambda_1 L_1(\phi)], \tag{43}$$

where ϕ is independent of η. The integrals (35) give

$$\left.\begin{aligned} I_1(\phi) &= -\phi\cos\phi + \frac{1}{2}\phi + \sin\phi - \frac{1}{2}\sin\phi\cos\phi \\ J_1(\phi) &= 2\phi - 2\sin\phi\cos\phi + \frac{4}{3}\sin^3\phi \\ K_1(\phi) &= \frac{1}{3}\sin^3\phi(1+\cos\phi) \\ L_1(\phi) &= \frac{1}{15}\sin^3\phi(1+\cos\phi)(6\cos\phi - 1) \end{aligned}\right\}. \tag{44}$$

The second derivative of the function f in square brackets in equation (43) is evaluated by means of Multhopp's interpolation polynomial

$$f(\eta) = (-1)^{(m-1)/2}\sum_{n=-(m-1)/2}^{(m-1)/2} f_n \frac{(-1)^{n+1}\sin(m+1)\theta\sin\theta_n}{(m+1)(\cos\theta - \cos\theta_n)}, \tag{45}$$

where $\eta = \cos\theta$, $\eta_n = \cos\theta_n = \sin\{n\pi/(m+1)\}$ and $f_n = f(\eta_n)$. Double differentiation and the substitution $\eta = \eta_\nu$ gives

$$\left(\frac{\partial^2 f}{\partial\eta^2}\right)_\nu = \sum_{n=-(m-1)/2}^{(m-1)/2} (-1)^{\nu-n} f_n \left\{\frac{\sin\theta_n \cos\theta_\nu}{\sin^3\theta_\nu(\cos\theta_\nu - \cos\theta_n)} - \frac{2\sin\theta_n}{\sin\theta_\nu(\cos\theta_\nu - \cos\theta_n)^2}\right\}, \tag{46}$$

where the coefficient of f_ν needs special care and is found to be

$$\frac{1}{\sin^2\theta_\nu}\left\{\frac{1}{3} - \frac{1}{3}(m+1)^2 + \cot^2\theta_\nu\right\}.$$

Since we are concerned with symmetrical spanwise loading, $f_{-n} = f_n$ and equation (46) gives

$$\left(\frac{\partial^2 f}{\partial\eta^2}\right)_\nu = \sum_{n=0}^{(m-1)/2} F_{\nu n} f_n, \tag{47}$$

where

$$\left.\begin{aligned}
F_{\nu 0}(\nu\neq 0) &= (-1)^\nu \left\{\frac{1}{(1-\eta_\nu^2)^{3/2}} - \frac{2}{\eta_\nu^2\sqrt{(1-\eta_\nu^2)}}\right\} \\
F_{\nu n}(\nu\neq n) &= (-1)^{\nu-n}\left\{\frac{2\eta_\nu^2\sqrt{(1-\eta_n^2)}}{(\eta_\nu^2-\eta_n^2)(1-\eta_\nu^2)^{3/2}} - \frac{(\eta_\nu^2+\eta_n^2)\,4\sqrt{(1-\eta_n^2)}}{(\eta_\nu^2-\eta_n^2)^2\,\sqrt{(1-\eta_\nu^2)}}\right\} \\
F_{\nu\nu}(\nu\neq 0) &= \frac{1}{2(1-\eta_\nu^2)} - \frac{1}{2\eta_\nu^2} + \frac{1}{1-\eta_\nu^2}\left\{\frac{1}{3} - \frac{1}{3}(m+1)^2 + \frac{\eta_\nu^2}{1-\eta_\nu^2}\right\} \\
F_{00} &= \frac{1}{3} - \frac{1}{3}(m+1)^2
\end{aligned}\right\}.$$

The required incidence at the collocation points

$$\alpha_{11}(\eta_\nu, \phi_p) = -\frac{1}{2\pi A}\left(\frac{\partial^2 f}{\partial\eta^2}\right)_\nu$$

is readily evaluated from values of f at the $\frac{1}{2}N(m+1)$ collocation points on the half wing. The function $F_{\nu n}$ is tabulated in Table 1 for $m = 7$, 11 and 15. Apart from some errors in computation, Gersten's coefficients A_{2n} in Table 4 of Ref. 2 are equivalent. For rectangular wings his method of calculation is essentially the same as the present one.

4.2. *Non-Rectangular Wings.*

The evaluation of equation (36) for other planforms is more complicated. It is simplest to regard f as a function of the two variables η and $-\frac{1}{2}\cos\phi$, so that by equation (37) the partial derivative

$$\left(\frac{\partial}{\partial\eta}\right)_{x=\text{const.}} = \left(\frac{\partial}{\partial\eta}\right)_{\phi=\text{const.}} - \frac{1}{c}\left\{\frac{dx_l}{d\eta} + \frac{1}{2}\frac{dc}{d\eta}(1-\cos\phi)\right\}\frac{\partial}{\partial(-\frac{1}{2}\cos\phi)}. \tag{48}$$

Then

$$\left(\frac{\partial f}{\partial\eta}\right)_{x=\text{const.}} = f', \text{ say,}$$

can be expressed in terms of ordinary derivatives

$$x_l' = \frac{dx_l}{d\eta},\; c' = \frac{dc}{d\eta},\; \left(\frac{c\gamma_1}{\bar{c}}\right)' = \frac{d}{d\eta}\left(\frac{c\gamma_1}{\bar{c}}\right),\; I_1' = \frac{dI_1}{d(-\frac{1}{2}\cos\phi)}, \text{ etc.}$$

Thus from the expression for f in equation (36)

$$f' = \left\{\left(\frac{c\gamma_1}{\bar{c}}\right)' I_1 + \left(\frac{c\mu_1}{\bar{c}}\right)' J_1 + \left(\frac{c\kappa_1}{\bar{c}}\right)' K_1 + \left(\frac{c\lambda_1}{\bar{c}}\right)' L_1\right\} -$$

$$- \tan\Lambda \left\{\frac{s\gamma_1}{\bar{c}} I_1' + \frac{s\mu_1}{\bar{c}} J_1' + \frac{s\kappa_1}{\bar{c}} K_1' + \frac{s\lambda_1}{\bar{c}} L_1'\right\}, \tag{49}$$

where

$$s \tan\Lambda = x_l' + \tfrac{1}{2}c'(1-\cos\phi)$$

and Λ is local angle of sweepback of the line ϕ = constant. I_1, J_1, K_1 and L_1 are defined in equation (44) and their derivatives with respect to $-\frac{1}{2}\cos\phi$ are

$$\left.\begin{aligned}
I_1' &= 2\int_0^\phi (1+\cos\phi')d\phi' &&= 2\phi + 2\sin\phi \\
J_1' &= 8\int_0^\phi (\cos\phi'+\cos 2\phi')d\phi' &&= 8\sin\phi + 4\sin 2\phi \\
K_1' &= 2\int_0^\phi (\cos 2\phi'+\cos 3\phi')d\phi' &&= \sin 2\phi + \frac{2}{3}\sin 3\phi \\
L_1' &= 2\int_0^\phi (\cos 3\phi'+\cos 4\phi')d\phi' &&= \frac{2}{3}\sin 3\phi + \frac{1}{2}\sin 4\phi
\end{aligned}\right\}. \tag{50}$$

The difficulties of the central kink of sweptback wings and Multhopp's use of an 'interpolated wing' in equation (22) are partly overcome by putting $f' = 0$ at the centre section $\eta = 0$; this follows from the smooth spanwise symmetry of the load distribution. To obtain numerical values of f' at the other collocation stations, the first term of equation (49) is evaluated by putting

$$f = P(|\eta|)\,(1-\eta^2)^q \text{ along } \phi = \text{constant}, \tag{51}$$

where P is a polynomial in $|\eta|$ having the required values P_n at

$$\eta = \eta_n = \sin\frac{n\pi}{m+1}\;[n = 0, 1, \ldots \tfrac{1}{2}(m-1)].$$

Then for $\eta \geqslant 0$

$$f = (1-\eta^2)^q \sum_{n=0}^{(m-1)/2} \left[P_n \prod_{t=0}^{(m-1)/2}{}' (\eta-\eta_t) \Big/ \prod_{t=0}^{(m-1)/2}{}' (\eta_n-\eta_t)\right],$$

where $\prod_{t=0}^{(m-1)/2}{}'$ denotes the product of the $\frac{1}{2}(m-1)$ values excluding that for $t = n$. It follows that at the collocation station $\eta = \eta_\nu (\nu \neq 0)$

$$\left(\frac{\partial f}{\partial \eta}\right)_{\phi=\text{const.}} = \sum_{n=0}^{(m-1)/2} G_{\nu n}^{(q)} f_n \tag{52}$$

with

$$\left.\begin{aligned}
G_{\nu\nu}^{(q)} &= -\frac{2q\eta_\nu}{1-\eta_\nu^2} + \sum_{n=0}^{(m-1)/2}{}' \frac{1}{\eta_\nu - \eta_n} \\
G_{\nu n}^{(q)} &= \left(\frac{1-\eta_\nu^2}{1-\eta_n^2}\right)^q \prod_{t=0}^{(m-1)/2}{}'' (\eta_\nu-\eta_t) \Big/ \prod_{t=0}^{(m-1)/2}{}' (\eta_n-\eta_t)
\end{aligned}\right\}, \tag{53}$$

where $\sum\limits_{n=0}^{(m-1)/2}{}'$ denotes that $n = \nu$ is not included in the summation and $\prod\limits_{t=0}^{(m-1)/2}{}''$ denotes that $t = n$ and $t = \nu$ are both omitted in the product. The value of q depends on the form of f near the tip and will normally be a multiple of $\frac{1}{2}$. With the aid of equation (49) we obtain

$$\left.\begin{aligned} f_\nu' &= \sum_{n=0}^{(m-1)/2} G_{\nu n}^{(q)} f_n - \bar{f}_\nu \tan \Lambda_\nu \quad (\nu \neq 0) \\ f_0' &= 0 \end{aligned}\right\}, \tag{54}$$

where

$$\left.\begin{aligned} f_n &= \left[\frac{c\gamma_1}{\bar{c}} I_1 + \frac{c\mu_1}{\bar{c}} J_1 + \frac{c\kappa_1}{\bar{c}} K_1 + \frac{c\lambda_1}{\bar{c}} L_1\right]_{\eta=\eta_n} \\ \bar{f}_\nu &= \left[\frac{s\gamma_1}{\bar{c}} I_1' + \frac{s\mu_1}{\bar{c}} J_1' + \frac{s\kappa_1}{\bar{c}} K_1' + \frac{s\lambda_1}{\bar{c}} L_1'\right]_{\eta=\eta_\nu} \\ s \tan \Lambda_\nu &= x_{l\nu}' + \tfrac{1}{2}c_\nu'(1-\cos\phi) \end{aligned}\right\}. \tag{55}$$

The second differential

$$f'' = \left(\frac{\partial f'}{\partial \eta}\right)_{\phi=\text{const.}} - \frac{s}{c} \tan \Lambda \frac{\partial f'}{\partial(-\frac{1}{2}\cos\phi)} \tag{56}$$

requires special care. We use the numerical definition of f' in equation (54) to evaluate the first term; for $\eta = 0$ the second term vanishes, but for $n \neq 0$ differentiation of equation (49) gives

$$\begin{aligned} \frac{\partial f'}{\partial(-\frac{1}{2}\cos\phi)} = &\left\{\left(\frac{c\gamma_1}{\bar{c}}\right)' I_1' + \left(\frac{c\mu_1}{\bar{c}}\right)' J_1' + \left(\frac{c\kappa_1}{\bar{c}}\right)' K_1' + \left(\frac{c\lambda_1}{\bar{c}}\right)' L_1'\right\} - \\ &- \frac{c'}{s}\left\{\frac{s\gamma_1}{\bar{c}} I_1' + \frac{s\mu_1}{\bar{c}} J_1' + \frac{s\kappa_1}{\bar{c}} K_1' + \frac{s\lambda_1}{\bar{c}} L_1'\right\} - \\ &- \tan\Lambda\left\{\frac{s\gamma_1}{\bar{c}} I_1'' + \frac{s\mu_1}{\bar{c}} J_1'' + \frac{s\kappa_1}{\bar{c}} K_1'' + \frac{s\lambda_1}{\bar{c}} L_1''\right\}. \end{aligned}$$

After some cancellation this may be written conveniently as

$$\left.\begin{aligned} \left[\frac{s}{c}\frac{\partial f'}{\partial(-\frac{1}{2}\cos\phi)}\right]_{\eta=\eta_\nu} = \bar{f}_\nu' &= \left[\frac{\partial \bar{f}}{\partial \eta}\right]_{\eta=\eta_\nu} - \bar{\bar{f}}_\nu \tan \Lambda_\nu \\ &= \sum_{n=0}^{(m-1)/2} G_{\nu n}^{(q')} \bar{f}_n - \bar{\bar{f}}_\nu \tan \Lambda_\nu \end{aligned}\right\}, \tag{57}$$

where $\bar{f}_n$ and $\tan \Lambda_\nu$ are defined in equation (55) and

$$\bar{\bar{f}}_\nu = \left[\frac{s^2\gamma_1}{c\bar{c}} I_1'' + \frac{s^2\mu_1}{c\bar{c}} J_1'' + \frac{s^2\kappa_1}{c\bar{c}} K_1'' + \frac{s^2\lambda_1}{c\bar{c}} L_1''\right]_{\eta=\eta_\nu} \tag{58}$$

with

$$\left.\begin{aligned} I_1'' &= 4 \cot \tfrac{1}{2}\phi \\ J_1'' &= 16(\cot \tfrac{1}{2}\phi - 2 \sin \phi) \\ K_1'' &= 4(\cot \tfrac{1}{2}\phi - 2 \sin \phi - 2 \sin 2\phi) \\ L_1'' &= 4(\cot \tfrac{1}{2}\phi - 2 \sin \phi - 2 \sin 2\phi - 2 \sin 3\phi) \end{aligned}\right\}. \tag{59}$$

Then equations (56) and (57) give

$$f_\nu'' = \sum_{n=0}^{(m-1)/2} G_{\nu n}^{(q'')} f_n' - \bar{f}_\nu' \tan \Lambda_\nu , \tag{60}$$

where f_n' is defined in equation (54), $\bar{f}_0' = 0$ and for $\nu \neq 0$ $\bar{f}_\nu'$ is defined in equation (57).

As remarked below equation (53), the values of q, q' and q'' in equations (54), (57) and (60) depend on the behaviour of the respective functions f, $\bar{f}$ and f' near the tip. As in the linear theory and implied in equation (45), γ_1, μ_1, κ_1 and λ_1 are supposed to be proportional to $\sqrt{(1-\eta^2)}$ as $\eta \to 1$, but the tip shape will affect the appropriate power q in equation (51) according to the following table:

Tip shape	c	q	q'	q''
Streamwise	$\neq 0$	$\frac{1}{2}$	$\frac{1}{2}$	$-\frac{1}{2}$
Parabolic	$\propto \sqrt{(1-\eta)}$	1	$\frac{1}{2}$	0
Triangular	$\propto (1-\eta)$	$1\frac{1}{2}$	$\frac{1}{2}$	$\frac{1}{2}$

The values of $G_{\nu n}^{(q)}$ for $q = -\frac{1}{2}, 0, \frac{1}{2}, 1, 1\frac{1}{2}$ are given in Table 2 for $m = 7$ and in Table 3 for $m = 11$. To obtain the values of

$$\alpha(x_{p\nu}, y_\nu) = \alpha_{11}(\eta_\nu, \phi_p) = -\frac{1}{2\pi A} f_\nu''(\phi_p), \tag{61}$$

it is necessary to substitute the appropriate values of ϕ_p from equation (23). The local sweepback is given by

$$s \tan \Lambda_\nu = x_{l\nu}' + \tfrac{1}{2} c_\nu' \left(1 - \cos \frac{2\pi p}{2N+1}\right). \tag{62}$$

The numerical quantities I_1, J_1, . . . for $N = 2$, 3 and 4, and their first and second derivatives I_1', I_1'', . . . are given in Table 4.

Unlike the procedure in Section 4.1, the present method of calculation for non-rectangular wings differs significantly from that used by Gersten[2]. The differences are considered in some detail in Section 6.2, where separate calculations for a constant-chord swept wing are discussed. By appealing to spanwise symmetry, such that $f_0' = \bar{f}_0' = 0$, we do not need to consider the values of Λ_0 at the centre section. In fact the 'interpolated wing' only enters explicitly into the evaluation of α_{11} through equation (54) and the dependence of f_0 on c_0. No rigorous treatment of the central kink is possible, but the procedure now adopted seems to be the safest.

4.3. *Summary of Methods.*

The non-linear theory of Section 3.2 involves the numerical procedures associated with Multhopp's linear theory and the evaluation of α_{11} from equation (36). Digital-computer programmes exist for converting linear equations (19) into a matrix equation

$$\{\alpha\} = [A]\{l\},$$

where $[A]$ is a square matrix of order $\frac{1}{2}N(m+1)$ in cases of spanwise symmetry. Thus the linear solution for the loading is given as

$$\{l_1\} = [A^{-1}]\{\alpha_1\}.$$

The additional computations for the non-linear theory involve a matrix operation

$$\{\alpha_{11}\} = [C]\{l_1\}$$

corresponding to equation (36) and finally the matrix product

$$\{l_{11}\} = [A^{-1}]\{\alpha_{11}\}.$$

In other words, by equation (32) the non-linear load distribution is

$$\{l\} = [A^{-1}]\{\alpha_1\}\alpha + [A^{-1}CA^{-1}]\{\alpha_1\}\alpha^2, \tag{63}$$

where $\{\alpha_1\}$ is a unit column corresponding to uniform incidence.

For rectangular wings the operation $[C]$ is formulated in Section 4.1 and reduces to

$$\alpha_{11}(\eta_\nu, \phi_p) = -\frac{1}{2\pi A}\sum_{n=0}^{(m-1)/2} F_{\nu n} f_{np}, \tag{64}$$

where

$$\begin{aligned} f_{np} &= (\gamma_1)_n I_1(\phi_p) + (\mu_1)_n J_1(\phi_p) + (\kappa_1)_n K_1(\phi_p) + (\lambda_1)_n L_1(\phi_p), \\ \phi_p &= 2\pi p/(2N+1); \end{aligned}$$

$F_{\nu n}$ is given in Table 1 for $m = 7$, 11 and 15, and $I_1(\phi_p)$, $J_1(\phi_p)$, ... are tabulated for integral values of $p = 1, \ldots N$ in Table 4.

For non-rectangular wings the corresponding operation in Section 4.2 is rather more complicated. A worked example is given in Appendix B to clarify the steps of the computation. Rearranged in order of computation, equations (54) to (62) become

$$\left.\begin{aligned}
\tan\Lambda_{\nu p} &= \frac{1}{s}\left[\frac{dx_l}{d\eta} + \tfrac{1}{2}\frac{dc}{d\eta}(1-\cos\phi_p)\right]_{\eta=\eta_\nu} \\
f_{\nu p} &= \frac{c_\nu}{\bar{c}}[(\gamma_1)_\nu I_1(\phi_p) + (\mu_1)_\nu J_1(\phi_p) + (\kappa_1)_\nu K_1(\phi_p) + (\lambda_1)_\nu L_1(\phi_p)] \\
\bar{f}_{\nu p} &= \frac{s}{\bar{c}}[(\gamma_1)_\nu I_1'(\phi_p) + (\mu_1)_\nu J_1'(\phi_p) + (\kappa_1)_\nu K_1'(\phi_p) + (\lambda_1)_\nu L_1'(\phi_p)] \\
\bar{\bar{f}}_{\nu p} &= \frac{s^2}{\bar{c}c_\nu}[(\gamma_1)_\nu I_1''(\phi_p) + (\mu_1)_\nu J_1''(\phi_p) + (\kappa_1)_\nu K_1''(\phi_p) + (\lambda_1)_\nu L_1''(\phi_p)] \\
&\left.\begin{aligned}
f_{\nu p}' &= \sum_{n=0}^{(m-1)/2} G_{\nu n}^{(q)} f_{np} - \bar{f}_{\nu p}\tan\Lambda_{\nu p} \\
\bar{f}_{\nu p}' &= \sum_{n=0}^{(m-1)/2} G_{\nu n}^{(q')} \bar{f}_{np} - \bar{\bar{f}}_{\nu p}\tan\Lambda_{\nu p}
\end{aligned}\right\} \nu = 1, 2, \ldots \tfrac{1}{2}(m-1) \\
f_{0p}' &= \bar{f}_{0p}' = 0 \\
\alpha_{11}(\eta_\nu, \phi_p) &= -\frac{1}{2\pi A}\left[\sum_{n=0}^{(m-1)/2} G_{\nu n}^{(q'')} f_{np}' - \bar{f}_{\nu p}'\tan\Lambda_{\nu p}\right]
\end{aligned}\right\}, \tag{65}$$

where $G_{\nu n}^{(q)}$ is given in Tables 2 and 3 for $m = 7$ and 11 respectively, q takes values q, q' and q'' according to tip shape (Section 4.2), and $I_1(\phi_p)$, $I_1'(\phi_p)$, $I_1''(\phi_p)$, etc. are tabulated for integral values of $p = 1, \ldots N$ in Table 4. Given $[A^{-1}]$ and $[A^{-1}]\{\alpha_1\}$, the last term of equation (63) can be calculated and checked on a desk machine in about $0{\cdot}01N^2(m+1)^2$ hours. That is to say, a non-linear solution for $m(N) = 11(3)$ will involve about 2 days' extra computation.

It should be noted that the method of calculation for non-rectangular wings does not reduce to that for rectangular wings when we substitute $\Lambda_{\nu p} = 0$. Equations (65) then become

$$\alpha_{11}(\eta_\nu, \phi_p) = -\frac{1}{2\pi A}\left[\sum_{n=1}^{(m-1)/2} G_{\nu n}^{(-1/2)} \left\{\sum_{r=0}^{(m-1)/2} G_{nr}^{(1/2)} f_{rp}\right\}\right] \tag{66}$$

instead of the more precise equation (64). However, the values of α_{11} from equations (64) and (66) only differ by at most $\frac{1}{4}\%$ of the mean value of α_{11}.

5. *Numerical Results.*

In order to apply the present method to any planform, it is first necessary to use Multhopp's[5] linear theory, as described in Section 3.1. This involves the choice of m, the number of collocation stations across the span, and N, the number of terms in the chordwise loading of equation (15). Having obtained from equations (19) the linear solution $\gamma_1, \mu_1, \ldots$ for a uniform unit incidence, we follow the procedure of equation (64) or (65) to evaluate α_{11}. It remains to obtain the linear solution $\gamma_{11}, \mu_{11}, \ldots$ for $\alpha = \alpha_{11}$ and then the loading characteristics from equations (39) to (42).

Calculations have been made for eleven wings and five types of planform, as listed in Table 5. The rectangular, constant-chord and complete delta wings are adequately defined in Table 5. The gothic wings only differ in their semi-span $s = \frac{1}{2}A\bar{c}$; otherwise the planform is defined in equation (B1) of the worked example in Appendix B. The leading edge $x_l(\eta)$, chord $c(\eta)$ and semi-span of the ogee wing are defined by the equations

$$\left.\begin{aligned} \eta &= \tfrac{1}{2}\frac{x_l}{c_r} + \left(\frac{x_l}{c_r}\right)^2 - \tfrac{1}{2}\left(\frac{x_l}{c_r}\right)^5 \\ c &= c_r - x_l \\ s &= \tfrac{1}{4}c_r \end{aligned}\right\}, \tag{67}$$

where c_r denotes root chord. The lift and pitching moment, referred to the aerodynamic quarter-chord axis, are expressed as coefficients in equation (40), viz.

$$\left.\begin{aligned} C_L &= a_1\alpha + a_{11}\alpha^2 \\ C_m &= m_1\alpha + m_{11}\alpha^2 \end{aligned}\right\},$$

and the numerical values of a_1, m_1, a_{11} and m_{11} are given for each wing in Table 6.

For certain rectangular, gothic and delta wings the calculations have been carried out for more than one pair of values $m(N)$. As would be expected, the lift slope a_1 is not sensitive to the choice of $m(N)$ and m_1 shows only slight dependence; the results for $m(N) = 11(3)$ are presented graphically against aspect ratio in Fig. 2 to illustrate the effects of planform.

The tabulated values of a_{11} and m_{11} for rectangular wings show negligible dependence on N, but a_{11} has an important and systematic variation with m. The results by the present method, plotted in Figs. 3 and 4, all correspond to $N = 3$ and show the calculated effect of m. The dashed curves from Gersten's method are taken from Ref. 2 and appear to correspond to Truckenbrodt's[4] linear theory with $m = 15$. It should be noted that some of Gersten's published results are taken from earlier work (Ref. 9) involving a linear theory due to Scholz[10] for rectangular wings; for the sake of uniformity these results have been ignored. The comparisons between the dashed curves of a_{11} and m_{11} and the points ($\times$) from the present calculations for $m = 15$ are most satisfactory for the rectangular wings.

Less satisfactory is the lack of convergence of a_{11} in Fig. 3, as m is increased. There is, however, an analytical explanation, that the expansion of w in powers of $|z - z'|$ is not valid at the wing tip where the loading is not differentiable; the treatment of slender-wing theory in Section 7 avoids this difficulty. The approximation in equation (10) becomes increasingly inaccurate as the wing tip is approached, especially when the tip chord is non-zero. Since the outermost collocation station $\eta = \cos[\pi/(m+1)]$ approaches $\eta = 1$ as m is increased, there is probably an optimum value of m for which the solution is closest to what would be obtained on the basis of Gersten's mathematical model without the approximation implied by equation (10). The authors consider that $m = 11$ is the wisest choice for wings of moderately low aspect ratio, for which the results of the non-linear theory become important.

The dashed curve of a_{11} for delta wings in Fig. 3 is taken from Gersten's results for slightly cropped tips. But the apparent discrepancies between his curves and the results of the present method for swept wings are mainly due to the differences in the method of calculation, mentioned in Section 4.2 and to be discussed further in Section 6.2.

By equation (40) the ratio of incremental non-linear to linear lift is

$$\Omega = \frac{a_{11}\alpha^2}{a_1\alpha} = \left(\frac{a_{11}}{a_1}\right)\alpha\,, \tag{68}$$

where α is in radians. The ratio Ω is plotted against α (in degrees) for various rectangular, delta and gothic wings in Fig. 5. An incidence of 15° and aspect ratio $A = 1$ may be typical of the take-off and landing of future slender aircraft; then, whatever the type of planform, about one third of the lift force acting on the aircraft may well be associated with non-linear effects of flow separation.

The spanwise loadings and distributions of centre of pressure are calculated from equations (41) and (42) for four wings at $\alpha = 0$, 10° and 20° in Figs. 6 and 7. It will be seen later that these results are of greater validity for rectangular wings than for swept wings, when the rolling-up of vortex layers has a marked effect on the spanwise load distribution, if not on the total lift and pitching moment. It is found in Fig. 6 that the calculated spanwise loading of the gothic wing is least affected by non-linear lift. In Fig. 7, on the other hand, all wings show a marked rearward movement in local centre of pressure as the flow separates.

In Fig. 4 of Ref. 11, Thomas presents experimental data on non-linear pitching characteristics by plotting $\Delta\bar{x}$, the forward displacement of the centre of non-linear lift from the centre of linear lift, against $\bar{x}_0$, the linear aerodynamic centre. In the notation of the present method

$$\left.\begin{aligned} \bar{x}_0 &= x_0 - \frac{m_1\bar{\bar{c}}}{a_1} = \bar{\bar{x}}_l + \bar{\bar{c}}\left(\frac{1}{4} - \frac{m_1}{a_1}\right) \\ \bar{x}_1 &= x_0 - \frac{m_{11}\bar{\bar{c}}}{a_{11}} = \bar{\bar{x}}_l + \bar{\bar{c}}\left(\frac{1}{4} - \frac{m_{11}}{a_{11}}\right) \\ \Delta\bar{x} &= \bar{x}_0 - \bar{x}_1 = \bar{\bar{c}}\left(\frac{m_{11}}{a_{11}} - \frac{m_1}{a_1}\right) \end{aligned}\right\} \tag{69}$$

are particularly convenient parameters that may be evaluated from Tables 5 and 6. The quantity $\Delta\bar{x}/l$, where l is the chordwise extent of the planform, is plotted against x_0/l in Fig. 8 from the theoretical results for the eleven planforms. Although these results for rectangular wings are virtually independent of m, those for the gothic and delta wings ($A = 1$) differ significantly for $m = 7$ and

$m = 11$. The longitudinal characteristics range from extreme stability for the most slender rectangular wing to a slight pitch-up for the delta and ogee wings about a rearward linear aerodynamic centre. Corresponding experimental data are examined in Section 6.5.

6. *Comparisons with Experiment and Appraisal of Method.*

Before we consider the experimental data for the various types of planform, some general remarks may be helpful. It will appear that, provided leading-edge separation occurs well before maximum lift, the measured lift shows non-linear characteristics in accord with the present method. In practice this proviso sets an upper limit to aspect ratio, that is particularly restrictive when the leading edge is rounded and the wing is thick. The experimental data will be subdivided into four groups, denoted by different symbols

$$\left.\begin{array}{ll} \text{(i) from round-nosed, thick wings} & (\mathrm{O}) \\ \text{(ii) from sharp-edged, thick wings} & (\nabla) \\ \text{(iii) from round-nosed, thin wings} & (\Delta) \\ \text{(iv) from sharp-edged, thin wings} & (\times) \end{array}\right\}.$$

The last three groups provide experimental lift curves in good agreement with the present method, while the points (O) from the first group usually lie closer to the linear theoretical curve. Except as stated in footnotes, the experimental data correspond to Reynolds numbers between 10^6 and 6×10^6, based on aerodynamic mean chord.

The pitching moment, referred to the aerodynamic quarter-chord axis from equation (30), is a sensitive quantity that can seldom be estimated to close percentage accuracy; when linear theory is considered to be applicable, C_m is subject to significant effects of wing thickness. However, the present method will be seen to predict satisfactorily the non-linear trends. Often the displacements from experimental points (O) to points (∇, Δ or $\times$) correlate with the displacements from the linear to the non-linear theoretical curves.

Since the basic mathematical model of Fig. 1 has no physical justification, an appraisal of the present method cannot be divorced from experiment. Each type of planform is used to illustrate distinct facets. For rectangular wings the efficacy of the method extends to the spanwise distributions of lift and chordwise centre of pressure (Section 6.1). Results for a constant-chord swept wing (Section 6.2) serve to illustrate the differences between Gersten's original method and the present adaptation. The method can be applied to arbitrary planforms, and the curved-tip wings of Section 6.3 are the most general that we consider. For delta wings the calculated spanwise distribution of lift is seen to be unreliable, while the total lift and pitching moment are in satisfactory agreement with experiment (Section 6.4). Section 6.5 gives particular attention to the prediction of the centre of non-linear lift and the aerodynamic centre of wings with unswept trailing edges.

6.1. *Rectangular Wings.*

Gersten's mathematical model was originally conceived for rectangular wings[9] (1957). As explained in Section 4.1, the present method is then essentially the same as those of Gersten in Refs. 9 and 2, except that Multhopp's linear theory has replaced those of Scholz[10] and Truckenbrodt[4] respectively. We have varied the numbers of spanwise and chordwise terms, and the results in Section 5 are found to be dependent on the former, but hardly affected by the latter.

The solutions in Table 6 include aspect ratios $A = 4$, 2 and 1. As the upper diagram of Fig. 5 suggests, for $A = 4$ the non-linear terms are quite small up to incidences associated with maximum lift. For $A = 2$ the stall is delayed, and in Fig. 9 the curves of C_L against α and C_m are compared with experimental data from Refs. 12 and 13 for thickness/chord ratios $t/c = 0 \cdot 092$ and 0. This evidence favours the present calculations for $m = 11$ rather than $m = 7$. The non-linear lift and the trend in pitching moment are well predicted up to an incidence $\alpha = 14°$. The same remarks apply to the rectangular wing of aspect ratio $A = 1$ in Fig. 10, except that the theory now holds good up to $\alpha = 20°$. The points (O) from Ref. 12 for round-nosed, thick wings lie between linear and non-linear theory; on such wings only partial flow separation would be expected before the slope of the lift curve begins to decrease.

The calculated and measured spanwise distributions of normal force coefficient C_{NL} are plotted in Fig. 11 for $A = 1$ and $\alpha = 7 \cdot 8°$ and $19 \cdot 4°$. The points (O) lie closer to linear theory except near the tip, while those (Δ) for the thin wing of Ref. 13 straddle the results of the present method for $m = 7$, 11 and 15. One feature that commends the full curve for $m = 11$ is that it gives the correct spanwise location of the peak value of C_{NL} near the tip. The much sharper peak for $m = 15$ is unrealistic and reveals the manner of the divergence of a_{11}, discussed in Section 5. It is unwise to use the present method to satisfy flow conditions as near the tip as $\eta = 0 \cdot 981$, where the approximation of equation (10) exaggerates the deficit in downwash velocity at the wing. It will be seen in Section 7, that slender-wing theory can be applied satisfactorily to the mathematical model without this particular approximation.

The calculated and measured spanwise distributions of X_{cp}, the local centre of pressure, are given for $A = 1$ and various incidences in Fig. 12. The only important discrepancies are near $\eta = 0$, where for $\alpha = 14 \cdot 5°$ and $19 \cdot 4°$ the measured values from Ref. 13 exceed the calculated ones by $0 \cdot 06$. Just as for the spanwise loading in Fig. 11, throughout the span the present method gives a marked improvement on linear theory. Moreover, in Fig. 12b the distribution of X_{cp} is less sensitive to the choice of m than that of C_{NL} in Fig. 11.

6.2. *Constant-Chord Swept Wings.*

The present method of calculation for non-rectangular wings is described in Section 4.2. This differs from Gersten's procedure which amounts to a direct double differentiation of the expression in square brackets in equation (36) for $\eta > 0$. For a wing of constant chord and sweepback equation (36) with $N = 3$ becomes

$$\alpha_{11} = -\frac{1}{2\pi A}\frac{\partial^2}{\partial \eta^2}[\gamma_1 I_1(\phi) + \mu_1 J_1(\phi) + \kappa_1 K_1(\phi)] \tag{70}$$

and equation (37) becomes

$$-\tfrac{1}{2}\cos\phi = \frac{x}{c} - \tfrac{1}{2} - \tfrac{1}{2}A\eta\tan\Lambda, \tag{71}$$

where c and Λ are now independent of η. Therefore in the present notation Gersten would calculate for any value of η

$$\alpha_{11} = -\frac{1}{2\pi A}\frac{\partial}{\partial \eta}\left[\left\{\frac{\partial \gamma_1}{\partial \eta}I_1 + \frac{\partial \mu_1}{\partial \eta}J_1 + \frac{\partial \kappa_1}{\partial \eta}K_1\right\} - \tfrac{1}{2}A\tan\Lambda\{\gamma_1 I_1' + \mu_1 J_1' + \kappa_1 K_1'\}\right] \tag{72}$$

$$= -\frac{1}{2\pi A}\left[\left\{\frac{\partial^2 \gamma_1}{\partial \eta^2}I_1 + \frac{\partial^2 \mu_1}{\partial \eta^2}J_1 + \frac{\partial^2 \kappa_1}{\partial \eta^2}K_1\right\} - A\tan\Lambda\left\{\frac{\partial \gamma_1}{\partial \eta}I_1' + \frac{\partial \mu_1}{\partial \eta}J_1' + \frac{\partial \kappa_1}{\partial \eta}K_1'\right\} + \right.$$

$$\left. + \tfrac{1}{4}A^2\tan^2\Lambda\{\gamma_1 I_1'' + \mu_1 J_1'' + \kappa_1 K_1''\}\right]. \tag{73}$$

The differences arise, because linear theory fails to represent the central kink of a swept wing. A rigorous linear solution would lead to an expression in square brackets in equation (72) that by symmetry would vanish identically at $\eta = 0$. Our present method in Section 4.2 is an attempt to minimise cumulative errors from this defect of linear theory by insisting that first derivatives with respect to y should be replaced by zero at $\eta = 0$.

We now simulate Gersten's method by admitting non-zero values of f_0' and $\bar{f}_0'$ in Section 4.2. Thus, for wings of constant chord and sweepback equations (65) would give

$$\alpha_{11}(\eta_\nu, \phi_p) = -\frac{1}{2\pi A}\left[\sum_{n=0}^{(m-1)/2} G_{\nu n}^{(-1/2)} f_{np}' - \bar{f}_{\nu p}' \tan\Lambda\right], \tag{74}$$

where

$$\left.\begin{aligned} \bar{f}_{\nu p}' &= \sum_{n=0}^{(m-1)/2} G_{\nu n}^{(1/2)} \bar{f}_{np} - \bar{\bar{f}}_{\nu p} \tan\Lambda \\ f_{\nu p}' &= \sum_{n=0}^{(m-1)/2} G_{\nu n}^{(1/2)} f_{np} - \bar{f}_{\nu p} \tan\Lambda \end{aligned}\right\} [\nu = 0, 1, \ldots \tfrac{1}{2}(m-1)]$$

with

$$\left.\begin{aligned} \bar{\bar{f}}_{\nu p} &= \tfrac{1}{4}A^2[(\gamma_1)_\nu I_1''(\phi_p) + (\mu_1)_\nu J_1''(\phi_p) + (\kappa_1)_\nu K_1''(\phi_p)] \\ \bar{f}_{\nu p} &= \tfrac{1}{2}A[(\gamma_1)_\nu I_1'(\phi_p) + (\mu_1)_\nu J_1'(\phi_p) + (\kappa_1)_\nu K_1'(\phi_p)] \\ f_{\nu p} &= [(\gamma_1)_\nu I_1(\phi_p) + (\mu_1)_\nu J_1(\phi_p) + (\kappa_1)_\nu K_1(\phi_p)] \end{aligned}\right\}$$

and the functions of ϕ_p in Table 4. As for rectangular wings, Gersten's differentiations in equation (73) follow from the interpolation polynomial of equation (45); apart from minor numerical differences this would appear to be consistent with $\alpha_{11}(\eta_\nu, \phi_p)$ as given above. The major effect of using Gersten's method or equation (74) in place of our present method in Section 4.2 is to introduce large changes in the distribution of α_{11} along the centre section. There are minor differences for $\nu \neq 0$, since f_0' is no longer zero, as defined in equation (54) and the first term of the summation in equation (74) contributes a little.

The implications have been examined for $A = 2$ and $\Lambda = 45°$; in Fig. 3 the non-linear lift according to our present method with $m = 11$ is given by $a_{11} = 1\cdot93$ and Gersten's corresponding value with $m = 15$ is $a_{11} = 1\cdot08$, reproduced from Fig. 8 of Ref. 2. Since a direct comparison for the same m is not available, we have constructed from Multhopp's linear solution for $m(N) = 11(3)$ and equation (74) what is to all intents and purposes a solution of 'Gersten's theory ($m = 11$)' giving

$$\left.\begin{aligned} C_L &= 2\cdot292\alpha + 0\cdot77\alpha^2 \\ C_m &= 0\cdot202\alpha - 0\cdot72\alpha^2 \end{aligned}\right\}, \tag{75}$$

where α is in radians. Just as for rectangular wings, the lower value $a_{11} = 0\cdot77$ for $m = 11$ would be expected. Similarly the non-linear pitching moment, given by $-m_{11} = 0\cdot72$, compares with the values $-m_{11} = 0\cdot51$ from our present method with $m = 11$ and $-m_{11} = 0\cdot87$ from Gersten's calculations with $m = 15$ (Fig. 4).

In Fig. 13, C_L and C_m from linear theory and the present method are compared with two sets of measurements on constant-chord wings with A = 2 and $\Lambda = 45°$. As usual, the round-nosed thick wing from Part II of Ref. 14 gives lift coefficients that lie well between linear and non-linear theory. The value $a_{11} = 1\cdot93$ from the present method supplies the non-linear lift measured on the sharp-edged thin wing* at incidences below the onset of the stall. The points ($\times$) on the graph of C_L against C_m are approximate only, but they undoubtedly show a similar but more marked non-linear trend than the present method. 'Gersten's theory ($m = 11$)' from equation (75) appears to give insufficient non-linear lift, but the curve of C_L against C_m is very satisfactory. Gersten gives further comparisons with experiment in Fig. 11 of Ref. 2 for a wing with $A = 1$ and $\Lambda = 45°$. So large is the increase in his value of a_{11} with decreasing aspect ratio that excellent predictions of lift and pitching moment are obtained.

The measurements of pressure distribution in Ref. 14 provide local normal-force coefficients C_{NL} which are plotted against η in Fig. 14. The round-nosed thick wing of moderate sweepback has only a part-span leading-edge vortex at $\alpha = 17 \cdot 3°$, and it is found that the spanwise distribution of C_{NL} follows close to linear theory except at the outermost station $\eta = 0 \cdot 87$. The present non-linear theory does not distinguish between C_{NL} and C_{LL} as defined in equation (41). The curve of large dashes labelled 'Gersten ($m = 15$)'** is in close agreement with the result of 'Gersten's theory ($m = 11$)' derived from Multhopp's linear solution and the quantity α_{11} in equation (74); the differences near the tip closely resemble those in the spanwise loadings of the rectangular wing for $m = 15$ and $m = 11$ in Fig. 11. The full curve from the present method probably represents fairly well the separated flow over the outer half of the wing. The increase in C_{NL} near the centre section is directly attributable to the mathematical model; this extra lift would have to be redistributed to satisfy a better physical model of the free vortex layers.

6.3. *Gothic and Ogee Wings.*

Gersten's non-linear theory, as formulated in Ref. 2, is restricted to wings with straight edges. The extension of his method of calculation to wings of curved planform would simply involve the inclusion of terms in $d^2c/d\eta^2$ and $d^2x_l/d\eta^2$. Without any modification the present method (Section 4.2) has been applied to gothic and ogee wings; a worked example for a gothic wing is set out in Appendix B.

Table 6 includes the solutions for gothic wings of aspect ratio $A = 1 \cdot 5$, $1 \cdot 0$, $0 \cdot 75$ and for the ogee wing defined in equations (67). Results for all three gothic wings have been calculated with $m = 7$; in order to make comparisons with available experimental data, these results have been interpolated and extrapolated with respect to A. Another solution for $A = 1$ with $m = 11$ confirms that for gothic wings the non-linear lift, as estimated with $m = 7$, is smaller than the preferred value with $m = 11$.

Experimental values of C_L for thick wings of gothic planform[15] are plotted against incidence in Fig. 15 to compare with linear and non-linear theory. For $A = 1 \cdot 092$ the points (O) for the elliptic-nosed section are much higher than linear theory and in fact agree with the present method ($m = 7$), whereas the points (∇) for the sharp-edged section are 15% higher and much closer to what would be calculated with $m = 11$. Values of C_L/A^2 and α/A, obtained by the slender-wing theory of Smith[16] for the $A = 1$ gothic planform of his family III are taken from Table 3 of Ref. 16 and used to provide a further theoretical curve in Fig. 15a; this lies considerably higher than the present method or any of the measured values. The effect of a body on the sharp-edged wing is to reduce

---

* The experimental data are due to K. Jacob; these are taken from Fig. 15 of Ref. 3 and correspond to a Reynolds number $0 \cdot 65 \times 10^6$.

** This is derived from Fig. 27 of Gersten's thesis (Institüt für Strömungsmechanik, T. H. Braunschweig, Bericht 59/30).

the measured C_L by about 8%. For the higher aspect ratio $A = 1 \cdot 732$ the non-linear theoretical contribution to the lift is smaller, and this is confirmed by the experimental points (+) for the two sharp-edged wings with body.

For the gothic planform $A = 1$, Fig. 16 shows that the non-linear lift curves for $m = 7$ and $m = 11$ agree satisfactorily with experimental results from Ref. 17 for a sharp-edged thin wing ($\times$). Measured values (∇) for a sharp-edged thick wing[18] show that the thickness effect is not important on C_L, but gives a consistent decrease in C_m over the incidence range. The values of C_m from experiment and the present method ($m = 11$) show a similar non-linear trend. For the more slender gothic planform $A = 0 \cdot 75$, Fig. 17 shows very satisfactory correlation between non-linear theory and experiments on a sharp-edged wing[19]; calculations for $m = 11$ would improve the theoretical lift curve and be unlikely to impair the excellent comparisons for C_L against C_m. In Fig. 18, experimental results from Ref. 20 for the ogee wing ($A = 1$) indicate that the present method again gives a good estimate of C_L. Measured values of C_m for the sharp-edged thick ogee wing are displaced from non-linear theory to the same extent as those for the gothic wing in Fig. 16. The slightly destabilizing (pitch-up) trend indicated by both non-linear theory and experiment for the ogee wing in Fig. 18 contrasts the corresponding stabilizing trend of C_m for the gothic wing of the same aspect ratio.

As we have already seen in Fig. 5, the calculated ratio of non-linear to linear lift increases with wing slenderness. This is confirmed in Fig. 19 by the consistent correlation between calculated and measured values of C_L against α for gothic wings of three different aspect ratios. The measured values[17] have been corrected for lower-surface bevel to give zero lift at zero incidence. The experimental points for $A = 1$ are also plotted as Wing 2 in Fig. 20a and show much better agreement with the present method for $m = 11$ than with the lower curve for $m = 7$.

6.4. *Delta Wings.*

The theoretical and experimental results for delta wings present a general picture similar to that for the curved-tip wings of Section 6.3. There is a remarkably close resemblance between Figs. 20a and 20b for the lift on gothic and delta wings of aspect ratio $A = 1$. Ref. 17 provides experimental results for thick wings (A and C), for thin wings (2A and 8A) with symmetrically bevelled edges, and for thin wings (2 and 8) with flat upper surfaces where corrections for lower-surface bevel give zero lift at zero incidence. The values lie systematically near the theoretical curves for $m = 7$ and $m = 11$ and help to establish the general applicability of the present method. Likewise we may compare Fig. 19 with Fig. 21, where the theoretical lift curves for three different aspect ratios, interpolated or extrapolated if necessary, are again supported by experiment (Ref. 17, Fig. 32). For the delta wings in Fig. 21 the calculations correspond to $m = 11$, and the comparisons are significantly better than for the gothic wings in Fig. 19 where $m = 7$ is used. Decrease in the aspect ratio of delta wings from $1 \cdot 6$ to $1 \cdot 0$ is seen to give a marked increase in non-linear lift.

Further comparisons in Figs. 22 to 24 include experimental results for the four types of wing section (Refs. 15, 17, 21 to 24*). While the measured values of C_L for round-nosed thick wings (O) correlate better with linear theory, the other experimental results ($\nabla \Delta \times$) all lie close to non-linear theory. It would appear from Fig. 23 that for a round-nosed thick wing the effect of a body is to increase the measured lift coefficient, and perhaps to stimulate leading-edge flow separation.

---

* The experimental data from Refs. 24 and 26 correspond to a Reynolds number $0 \cdot 7 \times 10^6$, based on aerodynamic mean chord.

The opposite tendency was observed on a sharp-edged gothic wing with and without body in Fig. 15a. Comparisons of C_m against C_L are also made in Figs. 22 to 24 for three delta wings ($A = 1 \cdot 5,\ 1 \cdot 456,\ 1 \cdot 0$). The measured values of C_m for round-nosed thick wings (O) appear considerably to the left of linear theory, while for other sections ($\nabla \Delta \times$) they tend to the right of linear theory and lie fairly close to the results of the present method for $m = 11$; the curve for $m = 7$ in Fig. 24 is less satisfactory.

The additional curve of C_L against α in Fig. 23 is calculated for $t/c = 0$ from an empirical expression for delta wings due to Bergesen and Porter[25] (1960)

$$C_L = \frac{2\pi A\alpha}{pA + 2} + 0 \cdot 0925\epsilon^2 - 0 \cdot 0146\epsilon - (0 \cdot 529\alpha - 0 \cdot 034)\left(\frac{t}{c}\right)^{1/2}, \tag{76}$$

where p is the ratio of wing semi-perimeter to wing span and

$$\epsilon = \alpha/\tan^{-1}(\tfrac{1}{4}A).$$

This formula is based on a flow investigation of the leading-edge vortices from a sharp-edged delta wing of aspect ratio $A = 1$, in which an attempt was made to correlate the non-linear lift with measured loci of the vortex cores. In fact the magnitude of the non-linearity in C_L was shown to be closely related to the vertical displacement of the vortex cores from the wing surface, but to be independent of their spanwise location. Unless this were so, Gersten's mathematical model could hardly be expected to yield useful results for swept wings. In Ref. 25 the formula (76) is claimed to predict the experimental lift curves accurately for sharp-edged delta wings of various thicknesses with aspect ratio in the range $1 \leqslant A \leqslant 2$. For $t/c = 0$ and $A = 1 \cdot 456$ it underestimates the non-linear lift, as given by the present method and the measured values from Ref. 22.

Values of C_L against α are plotted in Fig. 25 for a more slender delta wing ($A = 0 \cdot 7$), and good agreement between experiment (Ref. 26*) and the present method is still found. For this aspect ratio it is interesting to compare the present method with the slender-wing theories of Mangler and Smith[27], Brown and Michael[28] and Küchemann[29], that take into account the leading-edge vortices. Like the values from Ref. 16 for the gothic wing in Fig. 15a, the theory of Brown and Michael, on which Ref. 16 is based, overestimates the lift; on the other hand Küchemann's slender-wing theory underestimates C_L. The model used by Mangler and Smith is the most elaborate and realistic physically. As seen in Fig. 25, the curve from the present method is slightly below that of Ref. 27, with the experimental points between them.

Typical distributions of spanwise loading, as calculated by the present method, are shown in Fig. 6. No confidence can be placed in the large and unrealistic increases in loading near the centre section of swept wings. Although the spanwise loading on delta wings by the present method is not checked against experiment, Fig. 26 shows how widely the distributions for an $A = 1$ delta wing differ from the best available theoretical results from Fig. 6 of Ref. 27. There remains unsolved the theoretical problem of estimating satisfactorily the non-linear spanwise loading for wings of arbitrary planform.

6.5. *Aerodynamic Centres.*

As discussed in Section 5, Fig. 8 is a convenient representation of the pitching characteristics predicted by the present method. For gothic, ogee and delta wings the chordwise extent of the model is simply c_r, and the locations of the centres of linear and non-linear lift are represented

* See footnote on opposite page.

respectively by $\bar{x}_0/c_r$ and $\bar{x}_1/c_r$, as defined in equations (69). Some of the available tabulated measurements of C_L and C_m for sharp-edged thin and thick wings have been analysed to give the values of $\bar{x}_0/c_r$ and $\bar{x}_1/c_r$ in Table 7, where the sources of data are quoted. In Fig. 27, the quantity $\Delta\bar{x}/c_r = (\bar{x}_0 - \bar{x}_1)/c_r$ is plotted against $\bar{x}_0/c_r$, and different symbols are used to indicate the type of planform and whether the values are derived from the present method ($m = 11$) or from experiments on thin or thick wings. In the analysis of experimental data presented in Ref. 11, an approximately linear relationship is indicated between the quantities $\Delta\bar{x}$ and $\bar{x}_0$; the straight line in Fig. 27 is taken from Fig. 4 of Ref. 11 and corresponds to planforms with streamwise tips (e.g. gothic and ogee wings). The present analysis supports the linear relationship between $\Delta\bar{x}$ and $\bar{x}_0$.

All the results for gothic wings in Fig. 27 indicate an appreciable nose-down pitching moment due to leading-edge separation, while the experimental results for thin delta wings show nose-up pitching characteristics of similar severity, again in accord with Ref. 11. The smallest movement in aerodynamic centre occurs on the ogee wing; the optimum design might be achieved with a planform having an unswept trailing edge and a theoretical centre of linear lift in the range $0\cdot 55c_r < \bar{x}_0 < 0\cdot 60c_r$.

An empirical approach has been used by Devenish and Fry[30] to provide methods of predicting the aerodynamic centre

$$x_{ac} = x_0 - \bar{\bar{c}}\,\frac{\partial C_m}{\partial C_L} \tag{77}$$

of slender configurations with sharp leading edges. For flat-plate wings of aspect ratio $A = 1$ with an unswept trailing edge x_{ac} corresponding to $C_L = 0\cdot 8$ at low speeds is given in Fig. 2 of Ref. 30 simply as a linear function of $\bar{c}/c_r$. For $C_L = 0\cdot 1$, x_{ac} is obtained similarly from Fig. 5 of Ref. 30, apart from a correction dependent on tip shape; this correction is very small for gothic and ogee wings, but delta wings require special treatment for $C_L = 0\cdot 1$. Figs. 2 and 5 of Ref. 30 are restricted to the range $0\cdot 4 < \bar{c}/c_r < 0\cdot 7$, but we have extrapolated the straight lines in Fig. 28 and make comparisons with results of the present method ($m = 11$) for four wings of aspect ratio $A = 1$. By equations (77) and (40)

$$\frac{x_{ac}}{c_r} = \frac{x_0}{c_r} - \frac{\bar{\bar{c}}(m_1 + 2m_{11}\alpha)}{c_r(a_1 + 2a_{11}\alpha)}, \tag{78}$$

where a_1, m_1, a_{11} and m_{11} are given in Table 6, x_0 corresponds to the aerodynamic mean quarter-chord axis in equation (30) and α is regarded as a function of C_L. The full and dashed lines for $C_L = 0\cdot 8$ and $0\cdot 1$ respectively show a satisfactory correlation with values of x_{ac}/c_r from equation (78) for gothic, ogee, delta and square planforms.

7. *Alternative Treatment for Slender Wings.*

The results of the present method for rectangular wings, as discussed in Section 6.1, suggest that the calculations fail to converge as m, the number of spanwise stations, increases. This divergence can be attributed to the approximate expansion in $|z - z'|$ for the upwash at the wing surface induced by an elementary planar vortex sheet inclined at the angle $\frac{1}{2}\alpha$ to the wing. When the simplifying assumptions of slender-wing theory are combined with Gersten's mathematical model of Fig. 1, the approximate expansion becomes unnecessary. An alternative treatment without collocation is then possible, and the results restore confidence in Gersten's mathematical model for rectangular wings. The treatment can be used to obtain closed expressions for the lift and pitching moment on any slender wing having a straight trailing edge.

Linearized slender-wing theory involves two-dimensional solutions for the velocity potential in transverse sections x = constant. We suppose that the trailing edge is unswept and that the local semi-span $s(x)$ satisfies $\partial s/\partial x \geqslant 0$. The resulting integral equation relates $\Delta\Phi$, the discontinuity in velocity potential across the wing at the transverse section, to the upwash distribution $w(y)$ at the wing; by equation (7) of Ref. 31

$$\frac{\partial}{\partial y}[\Delta\Phi] = \frac{2}{\pi\sqrt{[\{s(x)\}^2 - y^2]}}\int_{-s(x)}^{s(x)} \frac{w(y_1)\sqrt{[\{s(x)\}^2 - y_1^2]}}{y - y_1}\,dy_1\,. \tag{79}$$

In the linear problem $w(y) = -U\alpha$; since $\Delta\Phi$ vanishes for $y = \pm s(x)$, equation (79) gives for all $x(0 \leqslant x \leqslant c_r)$

$$\Delta\Phi(y) = 2U\alpha\sqrt{[\{s(x)\}^2 - y^2]}\,. \tag{80}$$

The corresponding load distribution is

$$l = \frac{2}{U}\frac{\partial(\Delta\Phi)}{\partial x} = \frac{4\alpha s(x)}{\sqrt{[\{s(x)\}^2 - y^2]}}\frac{\partial s}{\partial x}\,. \tag{81}$$

Equation (81) is taken as a first approximation to the wing loading in the alternative treatment of the non-linear problem. The model of separated flow will then give an upwash velocity $w(x, y, z)$ which is formulated quite simply for rectangular and delta wings in Sections 7.1 and 7.2 respectively. At the wing surface w will take values w_s, say, that differ from the quantity $-U\alpha$ imposed by the boundary condition (12) on a wing at uniform incidence. We therefore add to the linear solution a non-linear contribution corresponding to $w = -U\alpha - w_s$; this, it is assumed, can be computed approximately from the linear integral equation (79). Thus the non-linear solution for $w = -U\alpha$ is identified with the linear solution for $w = -2U\alpha - w_s$,

$$\frac{\partial}{\partial y}[\Delta\Phi] = \frac{2}{\pi\sqrt{[\{s(x)\}^2 - y^2]}}\int_{-s(x)}^{s(x)} \frac{-2U\alpha - w_s}{y - y_1}\sqrt{[\{s(x)\}^2 - y_1^2]}\,dy_1\,. \tag{82}$$

The total lift can be expressed as

$$L = \rho U\int_{-s}^{s}\Delta\Phi_t\,dy\,,$$

where $s = s(c_r)$ is the semi-span of the wing and $\Delta\Phi_t$ is the value of $\Delta\Phi$ from equation (82) at the trailing edge. Hence

$$C_L = \frac{LA}{2\rho U^2 s^2} = A\int_{-1}^{1}\frac{\Delta\Phi_t}{2Us}\,d\left(\frac{y}{s}\right), \tag{83}$$

where from equation (82)

$$\frac{\Delta\Phi_t}{2Us} = \int_{-s}^{y}\frac{1}{\pi s\sqrt{(s^2 - y_2^2)}}\left[\int_{-s}^{s}\frac{-2\alpha + \alpha_t(y_1)}{y_2 - y_1}\sqrt{(s^2 - y_1^2)}\,dy_1\right]dy_2 \tag{84}$$

with $\alpha_t(y_1)$ as the value of $-w_s(y_1)/U$ at the trailing edge. When the order of integration is changed, equation (84) becomes

$$\begin{aligned}\frac{\Delta\Phi_t}{2Us} &= \frac{1}{2\pi s}\int_{-s}^{s}[-2\alpha + \alpha_t(y_1)]\log_e\frac{s^2 - y_1 y - \sqrt{\{(s^2 - y_1^2)(s^2 - y^2)\}}}{s^2 - y_1 y + \sqrt{\{(s^2 - y_1^2)(s^2 - y^2)\}}}\,dy_1 \\ &= \frac{2\alpha}{s}\sqrt{(s^2 - y^2)} + \frac{1}{2\pi s}\int_{-s}^{s}\alpha_t(y_1)\log_e\frac{s^2 - y_1 y - \sqrt{\{(s^2 - y_1^2)(s^2 - y^2)\}}}{s^2 - y_1 y + \sqrt{\{(s^2 - y_1^2)(s^2 - y^2)\}}}\,dy_1\,.\end{aligned} \tag{85}$$

By equations (83) and (85)

$$
\begin{aligned}
C_L &= \pi A\alpha - \frac{A}{s^2}\int_{-s}^{s} \alpha_t(y_1)\sqrt{(s^2-y_1^2)}dy_1 \\
&= \pi A\alpha + \frac{A}{s^2}\int_{-s}^{s} \frac{w_s(c_r, y_1)}{U}\sqrt{(s^2-y_1^2)}dy_1 . \qquad (86)
\end{aligned}
$$

The pitching-moment coefficient about the axis $x = x_0$ is

$$
C_m = \frac{A}{\bar{\bar{c}}s}\int_0^{c_r}\int_{-s(x)}^{s(x)} (x_0 - x)\frac{\partial}{\partial x}\left[\frac{\Delta\Phi(x, y)}{2Us}\right] dy\, dx .
$$

Integration by parts gives

$$
\begin{aligned}
C_m &= \frac{A}{\bar{\bar{c}}s}\left[\int_{-s}^{s} (x_0 - c_r)\frac{\Delta\Phi(c_r, y)}{2Us} dy + \int_0^{c_r}\int_{-s(x)}^{s(x)} \frac{\Delta\Phi(x, y)}{2Us} dydx\right] \\
&= \frac{(x_0 - c_r)}{\bar{\bar{c}}} C_L + \frac{\pi A\alpha}{\bar{\bar{c}}}\int_0^{c_r}\left[\frac{s(x)}{s}\right]^2 dx + \\
&\quad + \frac{A}{\bar{\bar{c}}s^2}\int_0^{c_r}\int_{-s(x)}^{s(x)} \frac{w_s(x, y_1)}{U}\sqrt{[\{s(x)\}^2 - y_1^2]}dy_1 dx . \qquad (87)
\end{aligned}
$$

When $w_s(x, y_1)$ is replaced by $-\alpha U$ in equations (86) and (87), the expressions for C_L and C_m become consistent with linear slender-wing theory.

7.1. *Slender Rectangular Wings.*

The linear solution in equation (80) becomes

$$
\Delta\Phi = 2U\alpha\sqrt{(s^2 - y^2)} ,
$$

which is independent of chordwise position. Gersten's mathematical model is now a single vortex sheet from the leading edge at an angle $\frac{1}{2}\alpha$ above the wing surface. In the (x, y, z) system of co-ordinates defined in Fig. 1, the two-dimensional solution of Laplace's equation, which satisfies

$$
\left.\begin{aligned}
\Phi(y, \pm 0) &= \pm U\alpha\sqrt{(s^2 - y^2)} \text{ for } |y| \leqslant s \\
&= 0 \qquad\qquad\qquad\quad \text{for } |y| \geqslant s
\end{aligned}\right\} ,
$$

is

$$
\Phi(y, z) = U\alpha[-z + \sqrt{(r_1 r_2)}\sin\tfrac{1}{2}(\theta_1 + \theta_2)] , \qquad (88)
$$

where

$$
\left.\begin{aligned}
r_1^2 &= (s - y)^2 + z^2, \sin\theta_1 = z/r_1 \\
r_2^2 &= (s + y)^2 + z^2, \sin\theta_2 = z/r_2
\end{aligned}\right\} .
$$

It follows that the induced velocity in the z-direction at any point (y, z) is

$$
w(y, z) = \frac{\partial\Phi}{\partial z} = U\alpha\left[-1 + \frac{|z|(r_1 + r_2)^2}{2\sqrt{2}r_1 r_2\sqrt{(r_1 r_2 - y^2 + s^2 + z^2)}}\right] . \qquad (89)
$$

Now at the wing surface

$$
z = -x\sin\tfrac{1}{2}\alpha = -\tfrac{1}{2}\alpha x + O(\alpha^3) ,
$$

and to this order of accuracy the upwash normal to the wing surface is

$$
w_s(x, y) = w(y, -\tfrac{1}{2}\alpha x) .
$$

By equation (89)

$$w_s(x, y) = U\alpha[-1 + F(\eta, \zeta)], \tag{90}$$

where

$$\left.\begin{aligned} F(\eta, \zeta) &= \frac{\zeta(\rho_1+\rho_2)^2}{2\sqrt{2}\,\rho_1\rho_2\rho_3} \\ \rho_1^2 &= (1-\eta)^2 + \zeta^2 \\ \rho_2^2 &= (1+\eta)^2 + \zeta^2 \\ \rho_3^2 &= \rho_1\rho_2 - \eta^2 + 1 + \zeta^2 \\ \xi &= x/c_r \\ \eta &= y/s \\ \zeta &= \tfrac{1}{2}\alpha x/s = \alpha\xi/A \end{aligned}\right\}. \tag{91}$$

with

At the trailing edge $\xi = 1$; by equations (86), (90) and (91) the non-linear lift coefficient is given by

$$\frac{C_L}{A^2} = \frac{\alpha}{A}\left[\frac{1}{2}\pi + \int_{-1}^{1} F\left(\eta, \frac{\alpha}{A}\right)\sqrt{(1-\eta^2)}d\eta\right]. \tag{92}$$

Similarly by equations (87), (90) and (91) the pitching-moment coefficient for rectangular wings about the axis $x = x_0 = \frac{1}{4}c_r$ reduces to

$$C_m = -\tfrac{3}{4}C_L + \pi A\alpha + A\alpha\int_0^1\int_{-1}^1 [-1 + F(\eta, \zeta)]\sqrt{(1-\eta^2)}d\eta d\xi.$$

Hence

$$\begin{aligned} \frac{C_m}{A^2} &= -\frac{3}{4}\left(\frac{C_L}{A^2}\right) + \frac{\alpha}{A}\left[\frac{1}{2}\pi + \int_0^1\int_{-1}^1 F(\eta, \zeta)\sqrt{(1-\eta^2)}d\eta d\xi\right] \\ &= -\frac{3}{4}\left(\frac{C_L}{A^2}\right) + \frac{\pi\alpha}{2A} + \int_0^{\alpha/A}\int_{-1}^1 F(\eta, \zeta)\sqrt{(1-\eta^2)}d\eta d\zeta. \end{aligned} \tag{93}$$

Values of C_L and C_m are obtained by numerical integration of equations (92) and (93). If the integrand is tabulated at the Multhopp positions $\eta = \eta_n = \sin\{n\pi/(m+1)\}$, then

$$\begin{aligned} I(\zeta) &= \int_{-1}^1 F(\eta, \zeta)\sqrt{(1-\eta^2)}d\eta \\ &= \frac{2\pi}{m+1}\left[\frac{1}{2}F(0, \zeta) + \sum_{n=1}^{(m-1)/2} F(\eta_n, \zeta)(1-\eta_n^2)\right]. \end{aligned}$$

Thus

$$\left.\begin{aligned} \frac{C_L}{A^2} &= \frac{\alpha}{A}\left[\frac{1}{2}\pi + I\left(\frac{\alpha}{A}\right)\right] \\ \frac{C_m}{A^2} &= \frac{\alpha}{A}\left[\frac{1}{8}\pi - \frac{3}{4}I\left(\frac{\alpha}{A}\right)\right] + \int_0^{\alpha/A} I(\zeta)d\zeta \end{aligned}\right\}. \tag{94}$$

Calculations have been made with $m = 7$ and $m = 15$, and the values of C_L/A^2 and C_m/A^2 are given in Table 8 for $\alpha/A \leqslant 0{\cdot}4$. The more accurate calculations for $m = 15$ hardly differ from those for $m = 7$.

The values of C_L/A^2 are plotted against α/A and against C_m/A^2 in Fig. 29. Early attempts at analysing the non-linear effects for low-aspect-ratio wings were made on the basis of cross-flow drag theory. For example, Flax and Lawrence[32] (1951) suggest empirical formulae for the lift and pitching moment on rectangular wings with sharp leading edges. When the linear solution for slender wings is inserted, these empirical formulae give

$$\left.\begin{aligned} \frac{C_L}{A^2} &= \frac{1}{2}\pi\left(\frac{\alpha}{A}\right) + 3\left(\frac{\alpha}{A}\right)^2 \\ \frac{C_m}{A^2} &= \frac{1}{4}\left(\frac{C_L}{A^2}\right) - \left(\frac{\alpha}{A}\right)^2 \end{aligned}\right\} . \tag{95}$$

It is seen from the curves plotted in Fig. 29 that the values given by equations (95) compare quite well with those of the present theory.

The slender-wing theory can be used to indicate how the method of Section 4.1 diverges as m increases. Consider the approximate upwash as given in Section 2.3 by an expansion in $|z - z'|$, and apply equation (9) on the basis of slender-wing theory. For a slender rectangular wing, the linear load distribution is concentrated at the leading edge $x = 0$ and

$$\tfrac{1}{2}Ul(x, y) = \frac{\partial}{\partial x}[\Delta\Phi(x, y)] = 0 \text{ for } x > 0 .$$

Therefore equation (9) is replaced by

$$w(y, z) = w_0(y) - \tfrac{1}{2}|z|\frac{\partial^2}{\partial y^2}[\Delta\Phi(y)] , \tag{96}$$

where $\Delta\Phi(y)$ is the linear solution in equation (79). Thus

$$w_s(c_r, y) = w(y, -\tfrac{1}{2}\alpha c_r) = U\alpha\left[-1 + \left(\frac{\alpha}{A}\right)\frac{s^3}{(s^2 - y^2)^{3/2}}\right] ,$$

which diverges at the wing tips. Moreover according to equation (86) the lift coefficient would also diverge. Thus the combination of the expansion in equation (96) with exact slender-wing theory would be erroneous. Nevertheless by equation (89) it is apparent that $w(\pm s, z)$ is finite, and that the approximate expansion in z holds for points away from the tips. For this reason a collocation method can give a satisfactory solution, unless the solving points lie too close to the wing tips.

7.2. *Slender Delta Wings.*

The linear solution in equation (80) becomes

$$\Delta\Phi = 2U\alpha\sqrt{[\{s(x)\}^2 - y^2]} ,$$

where $s(x) = \frac{1}{4}Ax$. In Gersten's mathematical model the plane $x =$ constant $(0 < x < c_r)$ contains trailing vortex elements corresponding to part of the planform $0 < x_1 < x$. A typical element gives a discontinuity

$$\delta(\Delta\Phi) = \frac{\partial}{\partial x_1}(\Delta\Phi)\delta x_1 = \frac{UA\alpha}{2}\frac{s(x_1)}{\sqrt{[\{s(x_1)\}^2 - y^2]}}\delta x_1$$

across the plane $z = -\frac{1}{2}\alpha x_1$, the wing being represented by $z = -\frac{1}{2}\alpha x$. The corresponding complex velocity potential in the $Z = y + iz$ plane is

$$\delta W = \delta\Phi + i\delta\Psi = \frac{UA\alpha}{4} \frac{is(x_1)}{\sqrt{[Z_1^2 - \{s(x_1)\}^2]}} \delta x_1,$$

where $Z_1 = Z + i\frac{1}{2}\alpha x_1$. Therefore in the plane $x =$ constant the complex potential is

$$W = \Phi + i\Psi = \frac{UA\alpha}{4} \int_0^x \frac{is(x_1)}{\sqrt{[Z_1^2 - \{s(x_1)\}^2]}} dx_1. \tag{97}$$

Since

$$w(y, z) = \frac{\partial\Phi}{\partial z} = -\frac{\partial\Psi}{\partial y},$$

it follows that at the wing surface

$$\begin{aligned} w_s(x, y) &= w(y, -\tfrac{1}{2}\alpha x) \\ &= -\frac{UA\alpha}{4} \frac{\partial}{\partial y} \left[\int_0^x \mathrm{Im} \left\{\frac{is(x_1)}{\sqrt{[Z_1^2 - \{s(x_1)\}^2]}}\right\} dx_1\right], \end{aligned}$$

where $Z_1 = y - i\frac{1}{2}\alpha(x - x_1)$. This can be written as

$$w_s(x, y) = -U\alpha \frac{\partial}{\partial \eta} \left[\int_0^1 \mathrm{Im} \left\{\frac{i\xi}{\sqrt{\{(\eta - i\zeta)^2 - \xi^2\}}}\right\} d\xi\right], \tag{98}$$

where

$$\left.\begin{aligned} \xi &= s(x_1)/s(x) = x_1/x \\ \eta &= y/s(x) \\ \zeta &= \frac{\frac{1}{2}\alpha(x - x_1)}{s(x)} = \frac{2\alpha}{A}(1 - \xi) \end{aligned}\right\}.$$

It can be shown that

$$\mathrm{Im} \left\{\frac{i\xi}{\sqrt{\{(\eta - i\zeta)^2 - \xi^2\}}}\right\} = \frac{\sqrt{2}\,\xi\eta\zeta}{\rho_1\rho_2\rho_3}, \tag{99}$$

where

$$\left.\begin{aligned} \rho_1^2 &= (\eta - \xi)^2 + \zeta^2 \\ \rho_2^2 &= (\eta + \xi)^2 + \zeta^2 \\ \rho_3^2 &= \rho_1\rho_2 - \eta^2 + \xi^2 + \zeta^2 \end{aligned}\right\}.$$

By equations (86), (98) and (99) the non-linear slender-wing theory gives a lift coefficient

$$C_L = \pi A\alpha - A\alpha \int_{-1}^1 \sqrt{(1 - \eta^2)} \frac{\partial}{\partial \eta} \left[\int_0^1 \frac{\sqrt{2}\,\xi\eta\zeta}{\rho_1\rho_2\rho_3} d\xi\right] d\eta. \tag{100}$$

Integration by parts leads to

$$\frac{C_L}{A^2} = \frac{\alpha}{A}\left[\pi - 2\int_0^1\int_0^1 \frac{J(\xi, \eta, \alpha/A)}{\sqrt{(1 - \eta^2)}} d\xi d\eta\right], \tag{101}$$

where

$$J(\xi, \eta, \alpha/A) = \frac{\sqrt{2}\,\xi\eta^2\zeta}{\rho_1\rho_2\rho_3}.$$

The easiest way to show that equation (101) gives the correct linear solution is to write

$$\frac{2\eta\zeta}{\rho_3} = \bar{\rho}_3 = (\rho_1\rho_2 + \eta^2 - \xi^2 - \zeta^2)^{1/2};$$

then, as $\alpha/A \to 0$, $\zeta = 0$ and

$$\left.\begin{aligned} J(\xi, \eta) &= \frac{\xi\eta}{\sqrt{(\eta^2-\xi^2)}} \text{ when } \xi < \eta \\ &= 0 \qquad\qquad \text{when } \xi > \eta \end{aligned}\right\},$$

and hence

$$\begin{aligned} C_L &= A\alpha\left[\pi - 2\int_0^1 \frac{\eta}{\sqrt{(1-\eta^2)}}\int_0^\eta \frac{\xi}{\sqrt{(\eta^2-\xi^2)}}\,d\xi d\eta\right] \\ &= A\alpha\left[\pi - 2\int_0^1 \frac{\eta^2}{\sqrt{(1-\eta^2)}}\,d\eta\right] = \tfrac{1}{2}\pi A\alpha. \end{aligned}$$

The non-linear pitching-moment coefficient for the delta wing is given by equation (87) with $x_0 = \frac{1}{2}c_r$, $\bar{c} = \frac{2}{3}c_r$; by equations (98) and (99) it follows that

$$\begin{aligned} C_m = &-\frac{3}{4}C_L + \frac{1}{2}\pi A\alpha - \\ &-\frac{3A\alpha}{2c_r}\int_0^{c_r}\int_{-1}^1 \left(\frac{s(x)}{s}\right)^2 \sqrt{(1-\eta^2)}\,\frac{\partial}{\partial\eta}\left[\int_0^1 \frac{\sqrt{2}\,\xi\eta\zeta}{\rho_1\rho_2\rho_3}\,d\xi\right] d\eta dx. \end{aligned} \tag{102}$$

Since $s(x)/s = x/c_r$ and the integrations with respect to ξ, η are independent of x, it follows by comparison of equations (100) and (102) that

$$C_m = -\frac{3}{4}C_L + \frac{1}{2}\pi A\alpha + \frac{3}{2c_r}(C_L - \pi A\alpha)\int_0^{c_r}\left(\frac{x}{c_r}\right)^2 dx = -\frac{1}{4}C_L. \tag{103}$$

Values of C_L are obtained by numerical integration of equation (101) with the order of integration changed. If for a given value of α/A, the function $J(\xi, \eta, \alpha/A)$ is tabulated at

$$(\xi, \eta) = (\xi_p, \eta_n) = \left[\sin\left(\frac{p\pi}{m+1}\right), \sin\left(\frac{n\pi}{m+1}\right)\right]$$

for integral values of p and n up to $\frac{1}{2}(m+1)$, then

$$\frac{C_L}{A^2} = \frac{\alpha}{A}\left[\pi - \frac{2\pi^2}{(m+1)^2}\int_0^{(m+1)/2}\sqrt{(1-\xi_p{}^2)}\int_0^{(m+1)/2} J(\xi_p, \eta_n, \alpha/A)\,dndp\right]$$

and the integrations are effected by use of Simpson's rule. The function J was calculated for $m = 15$, but it was necessary to subdivide the interval in n in the neighbourhood of $n = p$; at worst for $\alpha/A \leqslant 0\cdot10$ and $p = 7$, J had to be calculated at sub-intervals of 1/8. Thus C_L/A^2 has been calculated for $\alpha/A \leqslant 0\cdot30$; the values are given in Table 8, together with C_m/A^2 as given by equation (103).

In the upper diagram of Fig. 30 the results of the present slender-wing theory are seen to give a much lower estimate of non-linear lift than the theory of Mangler and Smith[27]; perhaps this can be attributed to the fact that the rolling-up of vortices from a slender delta wing will influence the vertical as well as the spanwise location of the vorticity. All the theoretical results of C_m/A^2 against C_L/A^2 for slender delta wings collapse on to the linear curve in the lower diagram of Fig. 30. The results of the present method for finite aspect ratios $A = 0 \cdot 6538$ and 1 are also shown, and there is a consistent trend from marginal pitch-up to neutral longitudinal stability as the planform becomes slender.

8. *Concluding Remarks.*

The present investigation enables us to make a critical assessment of Gersten's[2] non-linear theory. There are two special simplifications inherent in the theory. The first introduces the mathematical vortex model of the flow illustrated in Fig. 1; there is no physical justification for this model, and its adoption rests on eventual comparisons between calculated and measured forces. The second simplification involves the expansion of w in powers of $|z - z'|$ in equation (7); this approximation becomes increasingly suspect as the wing tip is approached. Since the numerical solutions are obtained by collocation, this difficulty is avoided by restricting the number of spanwise stations $\eta = \eta_n = \sin [n\pi/(m+1)]$. The theory only applies to incompressible flow; an extension to compressible flow would certainly involve an empirical reduction in the angle $\frac{1}{2}\alpha$ between the plane of the wing and each elementary vortex sheet (Fig. 1).

For rectangular wings the present method is no more than a reformulation of Gersten's theory in terms of Multhopp's[5] lifting-surface theory. For straight-edged swept wings important modifications to Gersten's theory have been introduced in Section 4.2. The discussion in Section 6.2 illustrates the differences between Gersten's original method and the present adaptation. While Gersten has not yet formulated his method for wings of curved planform, the present method is applied to such wings with little extra effort.

Most aerodynamic research groups will have access to a high-speed digital computer and mechanized programmes for linear lifting-surface calculations including Multhopp's theory. The non-linear solution is given in matrix form in equation (63). Given the basic matrix $[A^{-1}]$ and the linear solution $[A^{-1}]\{\alpha_1\}\alpha$, the non-linear increment can be calculated and checked on a desk machine in about $0 \cdot 01\ N^2(m+1)^2$ hours, e.g. 2 days' computation when $m(N) = 11(3)$. A worked example is given in Appendix B.

In general the calculated lift curves are in good agreement with experimental results, provided that either the thickness is small or the leading edge is sharp. For round-nosed thick wings the measured lift lies well between linear and non-linear theory, as fully separated flow develops only at high incidences. Although the pitching moment is found experimentally to depend on wing thickness, on all wings the pitching-moment curves show the same non-linear trends as experiment. For thin wings ($t/c \leqslant 0 \cdot 05$) the present method gives a decisive improvement on linear theory in all the cases considered (Figs. 9, 10, 13, 16, 17, 22, 23, 24).

For rectangular wings the non-linear lift becomes significant at incidences below maximum lift, provided that the aspect ratio $A < 3$, say. The comparisons with experiment show that the present method gives realistic estimates of the spanwise distributions of lift and local centre of pressure on a thin wing of square planform (Figs. 11 and 12). Some lack of convergence near the wing tip is discerned in Fig. 11, as m is increased up to 15.

On the untapered wings the non-linear lift is associated with a marked nose-down pitching moment about the linear aerodynamic centre. Planform taper reduces this effect and even reverses it for delta wings which show an appreciable nose-up instability. Theoretically and experimentally the longitudinal characteristics of the ogee wing come nearest to neutral stability, which might be expected for a planform whose theoretical linear aerodynamic centre lies between 0·55 and 0·60 root chord (Fig. 27).

For a delta wing of aspect ratio 0·7 the present method predicts a lift curve in good agreement with experiment and with the slender-wing theory of Mangler and Smith (Fig. 25). However, Gersten's second simplification in equation (7) precludes the application of the present method as a slender-wing theory (Section 7.1). Nevertheless it is explained in Section 7 how a slender-wing theory can be developed on the basis of Gersten's mathematical model without his second simplification, so as to avoid the divergence in upwash near the wing tips. This divergence does not appear to upset the general collocation method, if the number of spanwise terms is restricted to $m = 11$ so that the upwash is only calculated for $|\eta| \leqslant 0{\cdot}966$.

There are other possible sources of error in the present method:

(i) the unrealistic representation of the singularities at flow separation (Section 2.1),

(ii) the choice $\frac{1}{2}\alpha$ for the angular displacement of the trailing vorticity from the wing surface,

(iii) the lack of provision for the rolling-up of the vortex sheets into concentrated vortices,

(iv) the unsatisfactory treatment of the centre section of swept wings by linear theory, as it affects Section 4.2.

The success of the method for predicting the load distribution on rectangular wings suggests that the first source of error may be unimportant. The choice of angle $\frac{1}{2}\alpha$ is justified empirically by the comparisons between calculated and measured total lift and pitching moment for a range of planforms. The third and fourth sources of error are believed to be important for swept wings and to be responsible for the discrepancies illustrated in Fig. 26. There remains unsolved the theoretical problem of estimating satisfactorily the non-linear spanwise loading on non-slender, non-rectangular wings. Further development of the present method to incorporate the rolling-up of the elementary vortex sheets appears possible, and this might well reduce any uncertainties associated with the centre section.

The present work envisages the extension of the non-linear theory to the problem of unsteady flow past a wing of arbitrary planform in slow pitching motion about a high mean incidence. It follows from equation (40) that the pitching stiffness derivative is given by

$$\frac{\partial C_m}{\partial \alpha} = m_1 + 2m_{11}\alpha .$$

The extended theory (Ref. 6) also determines the pitching damping derivative as a linear function of α.

9. *Acknowledgements.*

Most of the linear solutions were calculated by the DEUCE Section of the Mathematics Division, N.P.L. The authors also acknowledge the assistance of Mrs. S. Lucas, who was responsible for the desk calculations. Miss J. M. Reynolds helped to prepare the tables and figures.

LIST OF SYMBOLS

a_1, a_{11}		Linear, non-linear lift defined in equation (40)
A		Aspect ratio of planform ($= 4s^2/S$)
$c(y)$		Local chord of wing
c'	$=$	$dc/d\eta$
$\bar{c}$		Geometric mean chord ($= S/2s$)
$\bar{\bar{c}}$		Aerodynamic mean chord in equation (29)
c_r		Root chord of wing
C_L		Lift coefficient ($= L/\frac{1}{2}\rho U^2 S$)
C_{LL}	$=$	(Lift per unit span)$/\frac{1}{2}\rho U^2 c = 4s\gamma/c$
C_m	$=$	(Pitching moment about $x = x_0$)$/\frac{1}{2}\rho U^2 S\bar{\bar{c}}$
C_{NL}	$=$	(Normal force per unit span)$/\frac{1}{2}\rho U^2 c$
f		Function defined in equation (36)
f', f''	$=$	$(\partial f/\partial\eta)_{x=\mathrm{const.}}$, $(\partial^2 f/\partial\eta^2)_{x=\mathrm{const.}}$
$\bar{f}, \bar{\bar{f}}$	$=$	$\frac{s}{c}\,[\partial f/\partial(-\frac{1}{2}\cos\phi)]_{\eta=\mathrm{const.}}$, $\frac{s}{c}\,[\partial \bar{f}/\partial(-\frac{1}{2}\cos\phi)]_{\eta=\mathrm{const.}}$
$\bar{f}'$	$=$	$(\partial \bar{f}/\partial\eta)_{x=\mathrm{const.}}$
$F(\eta, \zeta)$		Function defined in equation (91)
$F_{\nu n}$		Factors for double differentiation in equation (47) and Table 1
$G_{\nu n}^{(q)}$		Differentiation factors in equation (53) and Tables 2 and 3 [q is explained in equation (51) and the table in Section 4.2.]
i, j, k, l		Influence functions corresponding to γ, μ, κ, λ, e.g. equation (18)
I_1, J_1, K_1, L_1		Functions of ϕ in equation (35) and Table 4
I_1', etc.		Functions of ϕ in equation (50) and Table 4
I_1'', etc.		Functions of ϕ in equation (59) and Table 4
J		Function defined in equation (101)
l		Non-dimensional wing loading in equation (15) ($= \Delta p/\frac{1}{2}\rho U^2$)
l_1, l_{11}		Linear, non-linear wing loading defined in equation (13)
L		Lift force on wing

m		Number of collocation stations across the wing span (odd integer)
m_1, m_{11}		Linear, non-linear pitching moment defined in equation (40)
M		Mach number of free stream
n		Integer (*see* η_n)
N		Number of terms in chordwise loading
Δp		Lift per unit area
s		Semi-span of wing
$s(x)$		Local semi-span of slender wing
S		Area of planform
t/c		Thickness/chord ratio of root section
u, v, w		x, y, z-components of velocity perturbation
U		Velocity of free stream
w_0		Upward induced velocity according to linear theory
w_s		Upward induced velocity in equation (90) or (98)
W		Complex potential in transverse plane x = const.
x, y, z		Rectangular co-ordinates in Fig. 1
x', y', z'		Co-ordinates of planar vortex sheet
x_0		Aerodynamic quarter-chord pitching axis in equation (30)
$\bar{x}_0$		Linear aerodynamic centre in equation (69)
$\bar{x}_1$		Centre of incremental non-linear lift in equation (69)
$\Delta\bar{x}$	=	$\bar{x}_0 - \bar{x}_1$
x_{ac}		Aerodynamic centre in equation (77)
$x_l(y)$		Leading edge of wing referred to root
x_l'	=	$dx_l/d\eta$
$\bar{\bar{x}}_l$		Aerodynamic mean leading-edge ordinate in equation (30)
X_{cp}		Local centre of pressure in equation (26)
X, Y		Co-ordinates for influence functions, e.g. equation (18)
$z(x, y)$		Surface of thin wing

α		Incidence of wing (in radians unless otherwise stated)
α_1, α_{11}		Unit incidence, incidence distribution in equation (33)
α_t		Value of $-w_s/U$ at the trailing edge
γ, μ, κ, λ		Functions of spanwise position in wing loading l
γ_1, etc.		Values of γ, etc., corresponding to $\alpha = \alpha_1$
γ_{11}, etc.		Values of γ, etc., corresponding to $\alpha = \alpha_{11}$
$(\gamma_n)_1$		Value of γ_1 at $\eta = \eta_n$
$(\gamma_n)_{11}$		Value of γ_{11} at $\eta = \eta_n$
Γ		Strength of vortex sheet
$\zeta(\xi)$		In Section 7.1, see equation (91); in Section 7.2, see equation (98)
η		Non-dimensional spanwise ordinate ($= y/s$)
η_n, η_ν	=	$\sin[n\pi/(m+1)]$, $\sin[\nu\pi/(m+1)]$ with $\lvert n\rvert$, $\lvert \nu\rvert = 0, 1, \ldots \frac{1}{2}(m-1)$
θ		Angular spanwise ordinate ($= \cos^{-1}\eta$)
Λ		Local angle of sweepback in equation (49)
Λ_T		Angle of sweepback of trailing edge
ν		Integer (*see* η_ν)
ρ		Density of free stream
ρ_1, ρ_2, ρ_3		In Section 7.1, see equation (91); in Section 7.2, see equation (99)
ϕ, ϕ'		Angular chordwise ordinate in equation (37), (16)
ϕ_p	=	$2\pi p/(2N+1)$ with $p = 1, 2, \ldots N$
Φ		Velocity-potential perturbation
$\Delta\Phi$		Discontinuity in Φ across the wing
Ψ		Stream function in transverse plane x = const.
n		Suffix denoting value at collocation station $\eta = \eta_n$
p		Suffix denoting value at chordwise location $\phi = \phi_p$
t		Suffix denoting value at trailing edge
ν		Suffix denoting value at collocation station $\eta = \eta_\nu$
νn		Double suffix denoting influence of station η_n on station η_ν

REFERENCES

No.	*Author(s)*	*Title, etc.*
1	W. Bollay	A non-linear wing theory and its application to rectangular wings of small aspect ratio. *Z. angew. Math. Mech.*, Vol. 19, pp. 21 to 35. 1939.
2	K. Gersten	Nichtlineare Tragflächentheorie insbesondere für Tragflügel mit kleinem Seitenverhältnis. *Ingen.-Arch.*, Vol. 30, pp. 431 to 452. 1961.
3	K. Gersten	Calculation of non-linear aerodynamic stability derivatives of aeroplanes. DFL (Braunschweig) Report 143. 1961. AGARD Report 342. 1961.
4	E. Truckenbrodt	Tragflächentheorie bei inkompressibler Strömung. *Jb. wiss. Ges. Flugtech. (Luftf.)*, pp. 40 to 65. 1953.
5	H. Multhopp	Methods for calculating the lift distribution of wings (Subsonic lifting-surface theory). A.R.C. R. & M. 2884. January, 1950.
6	H. C. Garner and D. E. Lehrian ..	Pitching derivatives for a gothic wing oscillating about a mean incidence. A.R.C. C.P. 695. February, 1963.
7	A. R. Curtis	Tables of Multhopp's influence functions. N.P.L. Mathematics Division Report Ma/21/0505. May, 1952.
8	K. W. Mangler and B. F. R. Spencer	Some remarks on Multhopp's subsonic lifting-surface theory. A.R.C. R. & M. 2926. August, 1952.
9	K. Gersten	Nonlinear airfoil theory for rectangular wings in incompressible flow. N.A.S.A. Re 3–2–59W. February, 1959. (Translation of *Z. Flugwiss.*, Vol. 5, No. 9, pp. 276 to 280. September, 1957.)
10	N. Scholz	Beiträge zur Theorie der tragenden Fläche. *Ingen.-Arch.*, Vol. 18, pp. 84 to 105. 1950.
11	H. H. B. M. Thomas	State of the art of estimation of derivatives. AGARD Report 339. April, 1961.
12	O. Holme	Measurements of the pressure distribution on rectangular wings of different aspect ratios. FFA (Stockholm) Report 37. 1950.
13	N. Scholz	Kraft und Druckverteilungsmessungen an Tragflächen kleiner Streckung. *ForschArb. IngWes.*, Vol. 16, pp. 85 to 92. 1949.
14	J. Weber, D. Küchemann and G. G. Brebner	Low-speed tests on 45-deg swept-back wings. A.R.C. R. & M. 2882. May, 1951.

No.	Author(s)	Title, etc.
15	Ph. Poisson-Quinton	Quelques problèmes aérodynamiques posés par l'avion de transport supersonique aux basses vitesses. *La Recherche Aéronautique*, No. 82. May/June, 1961.
16	J. H. B. Smith	A theory of the separated flow from the curved leading edge of a slender wing. A.R.C. R. & M. 3116. November, 1957.
17	D. H. Peckham	Low-speed wind-tunnel tests on a series of uncambered slender pointed wings with sharp edges. A.R.C. R. & M. 3186. December, 1958.
18	D. H. Peckham and S. A. Atkinson ..	Preliminary results of low speed wind tunnel tests on a gothic wing of aspect ratio $1 \cdot 0$. A.R.C. C.P. 508. April, 1957.
19	J. G. Wright	Low speed wind tunnel measurements of the oscillatory longitudinal derivatives of a gothic wing of aspect ratio $0 \cdot 75$. A.R.C. 24 357. April, 1962.
20	A. L. Courtney and A. O. Ormerod ..	Pressure-plotting and force tests at Mach numbers up to $2 \cdot 8$ on an uncambered slender wing of $p = \frac{1}{2}$, $s/c_0 = \frac{1}{4}$ (Handley Page Ogee). A.R.C. R. & M. 3361. May, 1961.
21	G. E. Bartlett and R. J. Vidal ..	Experimental investigation of influence of edge shape on the aerodynamic characteristics of low aspect ratio wings at low speeds. *J. Ae. Sci.*, Vol. 22, pp. 517 to 533. August, 1955.
22	J. A. Lawford and A. R. Beauchamp ..	Low-speed wind-tunnel measurements on a thin sharp-edged delta wing with 70° leading-edge sweep, with particular reference to the position of leading-edge-vortex breakdown. A.R.C. R. & M. 3338. November, 1961.
23	S. B. Berndt	Three component measurement and flow investigation of plane delta wings at low speeds and zero yaw. KTH (Stockholm) Aero. Tech. Note 4. 1949.
24	L. P. Tosti	Low-speed static stability and damping-in-roll characteristics of some swept and unswept low-aspect-ratio wings. N.A.C.A. Tech. Note 1468. October, 1947.
25	A. J. Bergesen and J. D. Porter ..	An investigation of the flow around slender delta wings with leading edge separation. Princeton University, Aero. Eng. Dept. Report 510. May, 1960.
26	P. T. Fink and J. Taylor	Some low speed experiments with 20 degree delta wings. A.R.C. 17 854. September, 1955. (See also *Z. Flugwiss.*, Vol. 4, 1956.)

REFERENCES—*continued*

No.	*Author(s)*	*Title, etc.*
27	K. W. Mangler and J. H. B. Smith ..	A theory of the flow past a slender delta wing with leading edge separation. *Proc. Roy. Soc.* A, Vol. 251, pp. 200 to 217. 1959.
28	C. E. Brown and W. H. Michael, Jr. ..	On slender delta wings with leading-edge separation. N.A.C.A. Tech. Note 3430. April, 1955.
29	D. Küchemann	A non-linear lifting-surface theory for wings of small aspect ratio with edge separations. A.R.C. 17 769. April, 1955.
30	D. M. Devenish and J. N. B. Fry ..	The prediction of the aerodynamic centre position and pitch-up of slender wings with sharp leading edges. A.R.C. 24 915. June, 1963.
31	H. Lomax and M. A. Heaslet ..	Linearized lifting-surface theory for swept-back wings with slender plan forms. N.A.C.A. Tech. Note 1992. December, 1949.
32	A. H. Flax and H. R. Lawrence ..	The aerodynamics of low aspect-ratio wings and wing-body combinations. Third Anglo-American Aeronautical Conference, Brighton. September, 1951.

APPENDIX A

Upwash Field for Small $(z - z')$

Let $\Phi(x, y, z)$ be the velocity potential of a vortex sheet in the plane $z = z'$ and of strength $\Gamma(x, y)$. Then by Laplace's equation the upwash gradient

$$\frac{\partial w}{\partial z} = \frac{\partial^2 \Phi}{\partial z^2} = -\frac{\partial^2 \Phi}{\partial x^2} - \frac{\partial^2 \Phi}{\partial y^2}. \tag{A1}$$

There are certain restrictions on $\Gamma(x, y)$, such that the derivatives $\partial w/\partial z$ and $\partial^2 w/\partial z^2$ exist on each side of the sheet. Let $\Phi_u(x, y)$ and $\Phi_l(x, y)$ denote Φ on the upper and lower surfaces of the sheet respectively. Then

$$\Gamma = \frac{\partial \Phi_u}{\partial x} - \frac{\partial \Phi_l}{\partial x} = 2\frac{\partial \Phi_u}{\partial x}, \tag{A2}$$

and hence

$$\Phi_u = \tfrac{1}{2}\int_{-\infty}^{x} \Gamma(x_0, y)dx_0 = -\Phi_l. \tag{A3}$$

Therefore from equations (A1) to (A3) the upwash gradients at the upper and lower surfaces are given by

$$\left(\frac{\partial w}{\partial z}\right)_u = -\frac{1}{2}\frac{\partial \Gamma}{\partial x} - \frac{1}{2}\frac{\partial^2}{\partial y^2}\left[\int_{-\infty}^{x} \Gamma(x_0, y)dx_0\right] = -\left(\frac{\partial w}{\partial z}\right)_l. \tag{A4}$$

If w_0 denotes the value of w in the plane $z = z'$, then in the neighbourhood of the vortex sheet

$$\begin{aligned} w(x, y, z) &= w(x, y, z') + |z - z'|\left(\frac{\partial w}{\partial z}\right)_u + O(z - z')^2 \\ &= w_0 - \tfrac{1}{2}|z - z'|\left\{\frac{\partial \Gamma}{\partial x} + \frac{\partial^2}{\partial y^2}\left[\int_{-\infty}^{x} \Gamma(x_0, y)dx_0\right]\right\} \end{aligned} \tag{A5}$$

by equation (A4). Let $\Gamma(x, y) = 0$ for $x > x_t$; then in the wake of the vortex sheet equation (A5) becomes

$$w(x, y, z) = w_0 - \tfrac{1}{2}|z - z'|\frac{\partial^2}{\partial y^2}\left[\int_{-\infty}^{x_t} \Gamma(x_0, y)dx_0\right]. \tag{A6}$$

If, however, $\Gamma(x, y) = 0$ for $x < x'$, then upstream of the vortex sheet the contribution of order $|z - z'|$ disappears.

APPENDIX B

Worked Example for Gothic Wing ($A = 1$)

We take $m(N) = 7(3)$, i.e.

$$\left.\begin{aligned} &\text{spanwise stations } \eta = \eta_n = \sin\frac{n\pi}{8}\ (n = 0, 1, 2, 3) \\ &\text{chordwise stations } \phi = \phi_p = \frac{2\pi p}{7} \quad (p = 1, 2, 3) \end{aligned}\right\}.$$

The gothic planform is defined by

$$\left.\begin{aligned} x_l &= \frac{3}{2}\bar{c}[1-\sqrt{(1-|\eta|)}] \\ c &= \frac{3}{2}\bar{c}\sqrt{(1-|\eta|)} \\ s &= \frac{1}{2}\bar{c} \end{aligned}\right\}. \tag{B1}$$

Then

$$\tan\Lambda \doteq \frac{1}{s}\left[\frac{dx_l}{d\eta} + \frac{1}{2}\frac{dc}{d\eta}\left(1 - \cos\frac{2\pi p}{7}\right)\right]$$

$$= \frac{9\bar{c}}{8c}\left[1 + \cos\frac{2\pi p}{7}\right].$$

n	η_n	$(x_l)_n/\bar{c}$	$c_n/\bar{c}$	$(\gamma_n)_1$	$(\mu_n)_1$	$(\kappa_n)_1$
0	0·00000	0·05358	1·44642	0·91133	−0·03580	−0·19904
1	0·38268	0·32146	1·17854	0·84373	+0·01434	−0·04596
2	0·70711	0·68821	0·81179	0·64843	+0·04420	+0·09498
3	0·92388	1·08615	0·41385	0·35329	+0·05966	+0·15337

p	$\cos\frac{2\pi p}{7}$
1	+0·62349
2	−0·22252
3	−0·90097

$(x_l)_0/\bar{c}$ and $c_0/\bar{c}$ are defined in equation (22) for an interpolated wing. $(\gamma_n)_1$, $(\mu_n)_1$ and $(\kappa_n)_1$ are given by the linear solution for $\alpha = 1$.

$$\left.\begin{aligned} f_\nu &= \frac{c_\nu}{\bar{c}}\left[(\gamma_\nu)_1 I_1(\phi_p) + (\mu_\nu)_1 J_1(\phi_p) + (\kappa_\nu)_1 K_1(\phi_p)\right] \\ \bar{f}_\nu &= \frac{s}{\bar{c}}\left[(\gamma_\nu)_1 I_1'(\phi_p) + (\mu_\nu)_1 J_1'(\phi_p) + (\kappa_\nu)_1 K_1'(\phi_p)\right] \\ \bar{\bar{f}}_\nu &= \frac{s^2}{\bar{c}c_\nu}\left[(\gamma_\nu)_1 I_1''(\phi_p) + (\mu_\nu)_1 J_1''(\phi_p) + (\kappa_\nu)_1 K_1''(\phi_p)\right] \end{aligned}\right\},$$

where the functions of ϕ_p are given in Table 4.

For $\nu = 0, f_0' = 0$ and $\bar{f}_0' = 0$.

For $\nu = 1, 2, 3,$

$$\left.\begin{aligned} f_\nu' &= \sum_{n=0}^{3} G_{\nu n}^{(q)} f_n - \bar{f}_\nu \tan\Lambda_\nu \\ \bar{f}_\nu' &= \sum_{n=0}^{3} G_{\nu n}^{(q')} \bar{f}_n - \bar{\bar{f}}_\nu \tan\Lambda_\nu \end{aligned}\right\},$$

where $G_{\nu n}^{(q)}$ is given in Table 2, $q = 1$, $q' = \frac{1}{2}$, and

$$\tan\Lambda_\nu = \frac{9\bar{c}}{8c_\nu}\left[1 + \cos\frac{2\pi p}{7}\right].$$

$$(\alpha_\nu)_{11} = \alpha_{11}(\eta_\nu, \phi_p) = -\frac{1}{2\pi A} f_\nu'',$$

where

$$f_\nu'' = \sum_{n=0}^{3} G_{\nu n}^{(q'')} f_n' - \bar{f}_\nu' \tan\Lambda_\nu \text{ with } q'' = 0.$$

ν	p	$\tan\Lambda_\nu$	f_ν	$\bar{f}_\nu$	$\bar{\bar{f}}_\nu$	f_ν'	$\bar{f}_\nu'$	f_ν''	$(\alpha_\nu)_{11}$
0	1		0·41327	1·2229	1·455	0·0000	0·000	−13·026	+2·073
1	1	1·54973	0·43548	1·4607	1·568	−2·5652	− 2·536	+ 1·103	−0·176
2	1	2·24986	0·29714	1·3734	1·602	−3·6588	− 4·129	3·616	−0·576
3	1	4·41327	0·11487	0·9932	1·536	−5·6469	−11·442	37·042	−5·895
0	2		2·79635	2·5110	0·656	0·0000	0·000	−21·018	3·345
1	2	0·74216	2·44296	2·4027	0·526	−4·2204	− 1·411	− 3·450	0·549
2	2	1·07744	1·46031	1·8849	+0·353	−5·6393	− 2·713	− 3·813	0·607
3	2	2·11349	0·49317	1·0863	−0·089	−8·0416	− 6·212	− 3·409	0·542
0	3		5·47661	2·8564	0·080	0·0000	0·000	−23·987	3·818
1	3	0·09453	4·48302	2·6436	0·096	−5·1956	− 1·188	− 6·536	1·040
2	3	0·13724	2·54252	2·0288	0·151	−7·2154	− 2·853	− 7·914	1·260
3	3	0·26920	0·79874	1·1048	0·168	−9·9216	− 6·970	−15·903	2·531

$(\gamma_n)_{11}$, $(\mu_n)_{11}$ and $(\kappa_n)_{11}$ are given by the linear solution for $\alpha = \alpha_{11}$.

n	$(\gamma_n)_{11}$	$(\mu_n)_{11}$	$(\kappa_n)_{11}$
0	1·924	−0·257	+0·071
1	1·298	−0·241	+0·183
2	0·916	−0·241	+0·390
3	0·595	−0·297	−0·726

By equations (29) and (30) the aerodynamic quarter-chord pitching axis is

$$x_0 = \bar{\bar{x}}_l + \tfrac{1}{4}\bar{\bar{c}},$$

where

$$\bar{\bar{x}}_l = 0\cdot375\bar{c}, \qquad \bar{\bar{c}} = 1\cdot125\bar{c}.$$

The coefficients

$$\left.\begin{aligned} C_L &= a_1\alpha + a_{11}\alpha^2 \\ C_m &= m_1\alpha + m_{11}\alpha^2 \end{aligned}\right\}$$

are evaluated from equations (27) and (31).

$\gamma_n = (\gamma_n)_1$	$\gamma_n = (\gamma_n)_{11}$
$\mu_n = (\mu_n)_1$	$\mu_n = (\mu_n)_{11}$
$a_1 = 1 \cdot 4364$	$a_{11} = 2 \cdot 385$
$-m_1 = 0 \cdot 0099$	$-m_{11} = 0 \cdot 438$

TABLE 1

Values of $F_{\nu n}$ from Equation (47)

$m = 7$	ν	$n = 0$	$n = 1$	$n = 2$	$n = 3$
	0	$-21 \cdot 0000$	$+25 \cdot 2346$	$-5 \cdot 6569$	$+1 \cdot 7934$
	1	$+13 \cdot 5140$	$-27 \cdot 2304$	$+16 \cdot 5754$	$-3 \cdot 5147$
	2	$-2 \cdot 8284$	$+19 \cdot 6368$	$-40 \cdot 0000$	$+26 \cdot 5027$
	3	$-11 \cdot 7206$	$+20 \cdot 4853$	$+19 \cdot 1117$	$-100 \cdot 7695$

$m = 11$	ν	$n = 0$	$n = 1$	$n = 2$	$n = 3$	$n = 4$	$n = 5$
	0	$-47 \cdot 6667$	$+57 \cdot 6782$	$-13 \cdot 8564$	$+5 \cdot 6569$	$-2 \cdot 6667$	$+1 \cdot 1096$
	1	$+29 \cdot 8000$	$-57 \cdot 9402$	$+34 \cdot 6446$	$-9 \cdot 0974$	$+3 \cdot 7350$	$-1 \cdot 4735$
	2	$-7 \cdot 6980$	$+38 \cdot 1604$	$-64 \cdot 4444$	$+41 \cdot 3692$	$-10 \cdot 0074$	$+3 \cdot 3232$
	3	$+2 \cdot 8284$	$-10 \cdot 2137$	$+48 \cdot 9898$	$-93 \cdot 3333$	$+62 \cdot 2254$	$-12 \cdot 8803$
	4	$+2 \cdot 6667$	$-3 \cdot 4376$	$-6 \cdot 9282$	$+79 \cdot 1960$	$-177 \cdot 3333$	$+121 \cdot 0132$
	5	$-49 \cdot 3959$	$+100 \cdot 1401$	$-102 \cdot 5268$	$+92 \cdot 2358$	$+94 \cdot 2449$	$-496 \cdot 7262$

$m = 15$	ν	$n = 0$	$n = 1$	$n = 2$	$n = 3$	$n = 4$	$n = 5$	$n = 6$	$n = 7$
	0	$-85 \cdot 0000$	$+103 \cdot 0772$	$-25 \cdot 2346$	$+10 \cdot 7753$	$-5 \cdot 6569$	$+3 \cdot 2144$	$-1 \cdot 7934$	$+0 \cdot 8112$
	1	$+52 \cdot 5178$	$-100 \cdot 9393$	$+59 \cdot 8663$	$-16 \cdot 3048$	$+7 \cdot 3951$	$-3 \cdot 9411$	$+2 \cdot 1304$	$-0 \cdot 9492$
	2	$-13 \cdot 5140$	$+63 \cdot 3323$	$-102 \cdot 2111$	$+64 \cdot 1680$	$-16 \cdot 5754$	$+7 \cdot 1659$	$-3 \cdot 5147$	$+1 \cdot 4966$
	3	$+6 \cdot 0534$	$-18 \cdot 4492$	$+70 \cdot 7570$	$-123 \cdot 2002$	$+79 \cdot 1040$	$-19 \cdot 8095$	$+7 \cdot 9605$	$-3 \cdot 1149$
	4	$-2 \cdot 8284$	$+7 \cdot 9844$	$-19 \cdot 6369$	$+91 \cdot 5975$	$-168 \cdot 0000$	$+110 \cdot 4785$	$-26 \cdot 5027$	$+8 \cdot 7554$
	5	$-0 \cdot 6244$	$+0 \cdot 0367$	$+5 \cdot 0979$	$-23 \cdot 3587$	$+135 \cdot 8645$	$-267 \cdot 2321$	$+180 \cdot 7915$	$-37 \cdot 5274$
	6	$+11 \cdot 7206$	$-22 \cdot 8904$	$+20 \cdot 4853$	$-12 \cdot 4616$	$-19 \cdot 1117$	$+236 \cdot 6253$	$-537 \cdot 7887$	$+369 \cdot 9658$
	7	$-124 \cdot 0197$	$+251 \cdot 5019$	$-261 \cdot 9681$	$+279 \cdot 0197$	$-297 \cdot 2893$	$+274 \cdot 7738$	$+297 \cdot 7539$	$-1\,556 \cdot 6293$

TABLE 2

Values of $G_{\nu n}^{(q)}$ from Equation (53) for $m = 7$

$q = -\frac{1}{2}$	ν	$n = 0$	$n = 1$	$n = 2$	$n = 3$
	0	−5·1097	+8·9828	− 5·0273	+ 0·9554
	1	−0·7602	−1·8687	+ 3·1876	− 0·4745
	2	+0·3978	−2·9807	+ 1·2977	+ 1·1454
	3	−1·2262	+7·1960	−18·5786	+13·8519

$q = 0$	ν	$n = 0$	$n = 1$	$n = 2$	$n = 3$
	0	−5·1097	+9·7229	− 7·1097	+2·4966
	1	−0·7023	−2·3170	+ 4·1648	−1·1454
	2	+0·2813	−2·2813	− 0·1165	+2·1165
	3	−0·4693	+2·9807	−10·0547	+7·5433

$q = \frac{1}{2}$	ν	$n = 0$	$n = 1$	$n = 2$	$n = 3$
	0	−5·1097	+10·5240	−10·0547	+6·5240
	1	−0·6488	− 2·7654	+ 5·4416	−2·7654
	2	+0·1989	− 1·7460	− 1·5307	+3·9108
	3	−0·1796	+ 1·2346	− 5·4416	+1·2346

$q = 1$	ν	$n = 0$	$n = 1$	$n = 2$	$n = 3$
	0	−5·1097	+11·3910	−14·2195	+17·0479
	1	−0·5994	− 3·2137	+ 7·1097	− 6·6762
	2	+0·1406	− 1·3364	− 2·9450	+ 7·2262
	3	−0·0687	+ 0·5114	− 2·9450	− 5·0740

$q = 1\frac{1}{2}$	ν	$n = 0$	$n = 1$	$n = 2$	$n = 3$
	0	−5·1097	+12·3296	−20·1094	+44·5483
	1	−0·5538	− 3·6620	+ 9·2893	−16·1177
	2	+0·0995	− 1·0228	− 4·3592	+13·3524
	3	−0·0263	+ 0·2118	− 1·5938	−11·3826

TABLE 3

Values of $G_{\nu n}^{(q)}$ from Equation (53) for $m = 11$

$q = -\frac{1}{2}$	ν	$n = 0$	$n = 1$	$n = 2$	$n = 3$	$n = 4$	$n = 5$
	0	−9·4679	+23·7769	−31·1280	+28·3477	−14·4626	+ 2·4927
	1	−0·6278	− 5·2970	+10·4864	− 7·2660	+ 3·3519	− 0·5533.
	2	+0·1285	− 1·6394	− 2·8938	+ 6·2185	− 2·1986	+ 0·3320
	3	−0·0706	+ 0·6848	− 3·7491	− 0·2687	+ 3·9318	− 0·4641
	4	+0·0922	− 0·8092	+ 3·3950	−10·0706	+ 5·2803	+ 1·9243
	5	−0·4300	+ 3·6146	−13·8737	+32·1658	−52·0709	+32·8890

$q = 0$	ν	$n = 0$	$n = 1$	$n = 2$	$n = 3$	$n = 4$	$n = 5$
	0	−9·4679	+24·6157	−35·9435	+40·0898	−28·9251	+ 9·6310
	1	−0·6064	− 5·5744	+11·6960	− 9·9255	+ 6·4753	− 2·0650
	2	+0·1113	− 1·4699	− 3·5605	+ 7·6161	− 3·8081	+ 1·1110
	3	−0·0499	+ 0·5013	− 3·0611	− 1·6829	+ 5·5605	− 1·2680
	4	+0·0461	− 0·4189	+ 1·9601	− 7·1210	+ 1·8162	+ 3·7174
	5	−0·1113	+ 0·9685	− 4·1463	+11·7735	−26·9539	+18·4694

$q = \frac{1}{2}$	ν	$n = 0$	$n = 1$	$n = 2$	$n = 3$	$n = 4$	$n = 5$
	0	−9·4679	+25·4840	−41·5040	+56·6955	−57·8502	+37·2115
	1	−0·5858	− 5·8518	+13·0452	−13·5585	+12·5094	− 7·7068
	2	+0·0964	− 1·3178	− 4·2271	+ 9·3278	− 6·5958	+ 3·7174
	3	−0·0353	+ 0·3670	− 2·4994	− 3·0971	+ 7·8637	− 3·4641
	4	+0·0230	− 0·2168	+ 1·1316	− 5·0353	− 1·6479	+ 7·1815
	5	−0·0288	+ 0·2595	− 1·2392	+ 4·3094	−13·9524	+ 4·0499

$q = 1$	ν	$n = 0$	$n = 1$	$n = 2$	$n = 3$	$n = 4$	$n = 5$
	0	−9·4679	+26·3830	−47·9246	+80·1795	−115·7004	+143·7739
	1	−0·5658	− 6·1292	+14·5501	−18·5213	+ 24·1662	− 28·7620
	2	+0·0835	− 1·1815	− 4·8938	+11·4242	− 11·4242	+ 12·4388
	3	−0·0249	+ 0·2687	− 2·0407	− 4·5113	+ 11·1210	− 9·4641
	4	+0·0115	− 0·1122	+ 0·6534	− 3·5605	− 5·1120	+ 13·8737
	5	−0·0074	+ 0·0695	− 0·3703	+ 1·5774	− 7·2223	− 10·3696

$q = 1\frac{1}{2}$	ν	$n = 0$	$n = 1$	$n = 2$	$n = 3$	$n = 4$	$n = 5$
	0	−9·4679	+27·3137	−55·3386	+113·3910	−231·4008	+555·4998
	1	−0·5466	− 6·4066	+16·2285	− 25·3005	+ 46·6856	−107·3411
	2	+0·0723	− 1·0593	− 5·5605	+ 13·9917	− 19·7873	+ 41·6210
	3	−0·0176	+ 0·1967	− 1·6662	− 5·9255	+ 15·7274	− 25·8564
	4	+0·0058	− 0·0581	+ 0·3772	− 2·5176	− 8·5761	+ 26·8019
	5	−0·0019	+ 0·0186	− 0·1107	+ 0·5774	− 3·7385	− 24·7892

TABLE 4

Values of Functions in Equations (44), (50) *and* (59)

N	p	ϕ_p	I_1	J_1	K_1	L_1
2	1	$2\pi/5$	1·044106	3·072474	—	—
2	2	$4\pi/5$	4·115468	6·248371	—	—
3	1	$2\pi/7$	0·427255	1·457471	0·258623	—
3	2	$4\pi/7$	2·380465	5·259814	0·240151	—
3	3	$6\pi/7$	4·401862	6·276326	0·002696	—
4	1	$2\pi/9$	0·210852	0·765568	0·156345	+0·112451
4	2	$4\pi/9$	1·354976	3·723990	0·373655	+0·003130
4	3	$6\pi/9$	3·176927	5·920841	0·108253	−0·086603
4	4	$8\pi/9$	4·523097	6·281186	0·000804	−0·001068

N	p	ϕ_p	I_1'	J_1'	K_1'	L_1'
2	1	$2\pi/5$	4·41539	9·95959	—	—
2	2	$4\pi/5$	6·20212	0·89806	—	—
3	1	$2\pi/7$	3·35886	10·15436	+1·26418	—
3	2	$4\pi/7$	5·54025	6·06389	−0·95510	—
3	3	$6\pi/7$	6·25336	0·34374	−0·13188	—
4	1	$2\pi/9$	2·68184	9·08153	+1·56216	+0·74836
4	2	$4\pi/9$	4·76214	9·24654	−0·23533	−0·89874
4	3	$6\pi/9$	5·92084	3·46410	−0·86603	+0·43301
4	4	$8\pi/9$	6·26909	0·16501	−0·06544	+0·08495

N	p	ϕ_p	I_1''	J_1''	K_1''	L_1''
2	1	$2\pi/5$	5·5055	− 8·4117	—	—
2	2	$4\pi/5$	1·2997	−13·6104	—	—
3	1	$2\pi/7$	8·3061	+ 8·2057	−5·7480	—
3	2	$4\pi/7$	3·1899	−18·4381	−1·1385	—
3	3	$6\pi/7$	0·9130	−10·2324	+3·6966	—
4	1	$2\pi/9$	10·9899	+23·3904	−2·0308	−12·4232
4	2	$4\pi/9$	4·7670	−12·4458	−5·8476	+ 4·5447
4	3	$6\pi/9$	2·3094	−18·4752	+2·3094	+ 2·3094
4	4	$8\pi/9$	0·7053	− 8·1234	+3·1114	− 7·2808

TABLE 5

Details of Eleven Planforms

Wing	A	Λ_T	$\bar{\bar{c}}/\bar{c}$	$c_r/\bar{c}$	$\bar{\bar{x}}_l/\bar{c}$	$x_0/\bar{c}$	Tip shape
Rectangular	1, 2, 4	0	1·00000	1·0	0	0·25000	$c \neq 0$
Constant chord	2	45°	1·00000	1·0	0·50000	0·75000	$c \neq 0$
Gothic	0·75, 1, 1·5	0	1·12500	1·5	0·37500	0·65625	$c \propto \sqrt{(1-\eta)}$
Ogee	1	0	1·23810	2·0	0·76190	1·07143	$c \propto \sqrt{(1-\eta)}$
Delta	0·6538, 1, 1·5	0	1·33333	2·0	0·66667	1·00000	$c \propto (1-\eta)$

TABLE 6

Solutions for Lift and Pitching Moment

Wing	A	$m(N)$	a_1	$-m_1$	a_{11}	$-m_{11}$
Rectangular	1·00	7(2)	1·458	−0·117	2·60	0·55
	1·00	7(3)	1·462	−0·124	2·66	0·55
	1·00	7(4)	1·460	−0·125	2·66	0·55
	1·00	11(3)	1·461	−0·122	3·17	0·66
	1·00	15(3)	1·461	−0·121	3·53	0·74
	2·00	7(2)	2·479	−0·105	1·75	0·32
	2·00	15(2)	2·475	−0·099	2·36	0·44
	4·00	7(2)	3·579	−0·075	0·94	0·15
Constant chord	2·00	11(3)	2·292	−0·202	1·93	0·51
Gothic	0·75	7(3)	1·115	0·009	2·59	0·55
	1·00	7(3)	1·436	0·010	2·38	0·44
	1·00	11(3)	1·426	0·037	3·09	0·42
	1·50	7(3)	1·998	0·007	2·01	0·29
Ogee	1·00	11(3)	1·392	0·162	2·74	0·27
Delta	$0{\cdot}65_4$	11(3)	0·922	0·158	3·67	0·48
	1·00	7(3)	1·338	0·179	1·85	0·07
	1·00	11(3)	1·327	0·206	2·47	0·28
	1·50	11(3)	1·829	0·247	1·42	0·09

TABLE 7

Centres of Linear and Non-Linear Lift from Experimental Data

Wing	A	t/c	$\bar{x}_0/c_r$	$\bar{x}_1/c_r$	Source of data
Gothic	0·75	0	$0·47_5$	$0·55_5$	Ref. 17 (Wing 1)
	0·75	0·050	0·50	0·54	*
	0·75	0·082	0·50	0·55	*
	1·00	0	$0·47_5$	0·52	Ref. 17 (Wings 2 & 2A)
	1·00	0·082	0·49	0·54	*
	1·00	0·120	$0·49_5$	$0·53_5$	Ref. 18 (Wing A)
	1·25	0	0·46	0·52	Ref. 17 (Wing 3)
Ogee	1·00	0·062	0·64	0·63	Ref. 19
Delta (rounded tips)	0·76	0	0·49	0·53	Ref. 17 (Wing 12)
	1·13	0	$0·53_5$	0·54	Ref. 17 (Wing 11)
Delta (pointed tips)	1·00	0	$0·60_5$	0·55	Ref. 17 (Wings 8 & 8A)
	1·00	0·082	0·60	0·54	*
	1·00	0·120	$0·64_5$	0·67	Ref. 17 (Wing C)
	1·33	0	$0·59_5$	$0·52_5$	Ref. 17 (Wing 9)
	1·67	0	$0·58_5$	$0·50_5$	Ref. 17 (Wing 10)

* Unpublished results from A. V. Roe and Co., Ltd.

TABLE 8

Solutions by Present Slender-Wing Theory

	Rectangular Wings				Delta Wings	
	$m = 7$		$m = 15$		$m = 15$	
$\frac{\alpha}{A}$	C_L/A^2	C_m/A^2	C_L/A^2	C_m/A^2	C_L/A^2	C_m/A^2
0·025	0·0419	—	0·0423	—	—	—
0·050	0·0885	0·0174	0·0887	0·0177	0·0833	−0·0208
0·100	0·1911	0·0327	0·1909	0·0332	0·1742	−0·0436
0·200	0·4221	0·0610	0·4221	0·0613	0·3785	−0·0946
0·300	0·6784	0·0875	0·6784	0·0879	0·6081	−0·1520
0·400	0·9524	0·1144	0·9524	0·1148	—	—

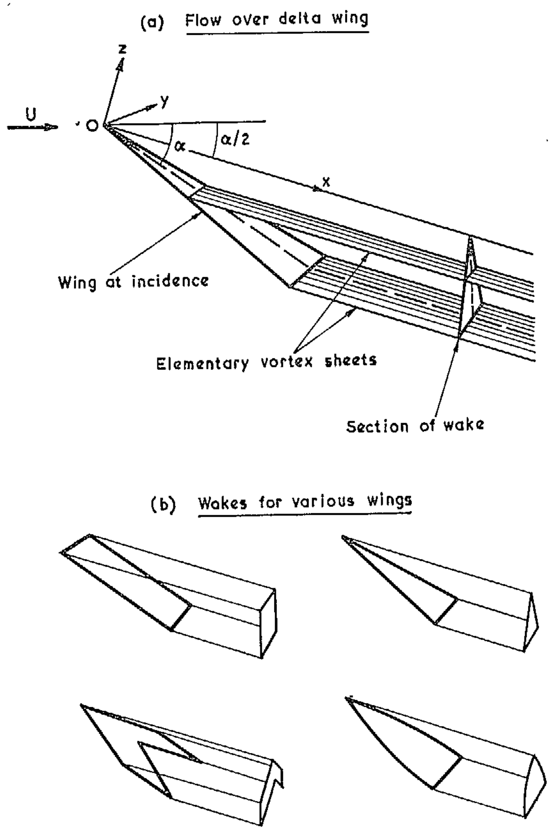

FIG. 1. Vortex model of flow over wings with leading-edge separation.

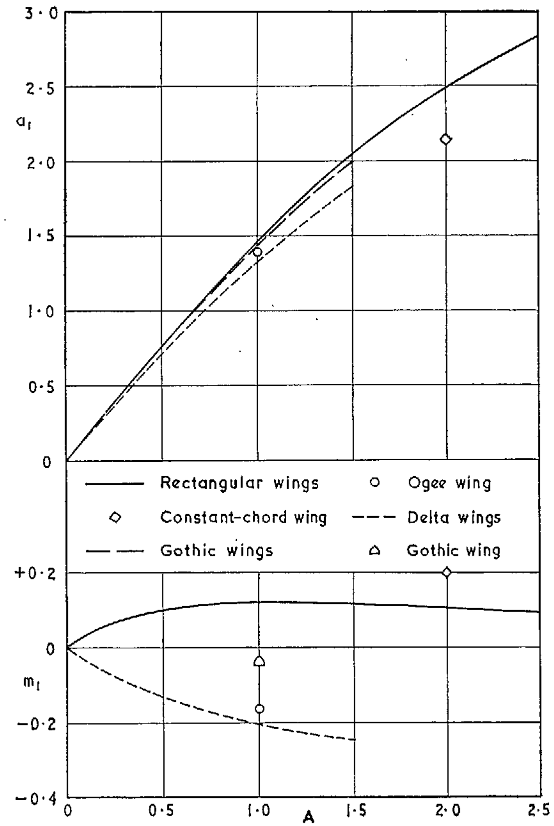

FIG. 2. Linear lift and pitching-moment slopes.

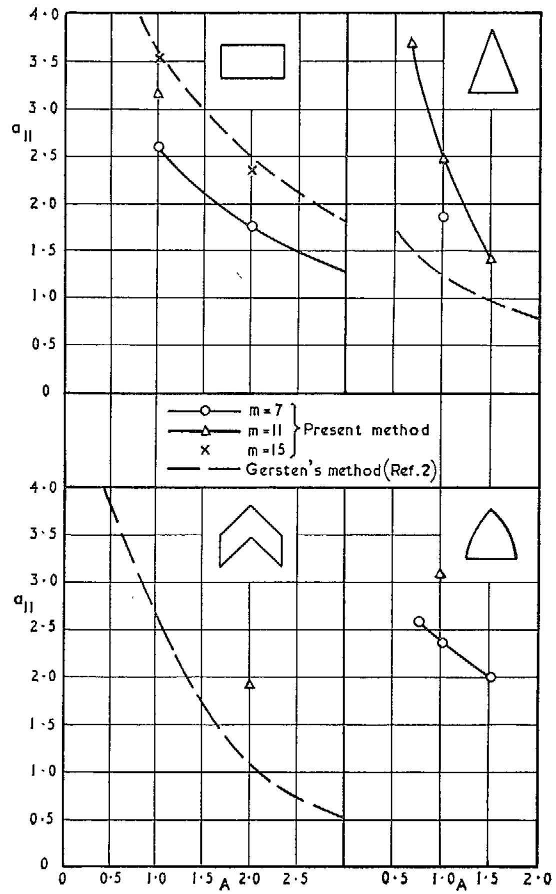

FIG. 3. Non-linear lift coefficient $(= a_{11}\alpha^2)$.

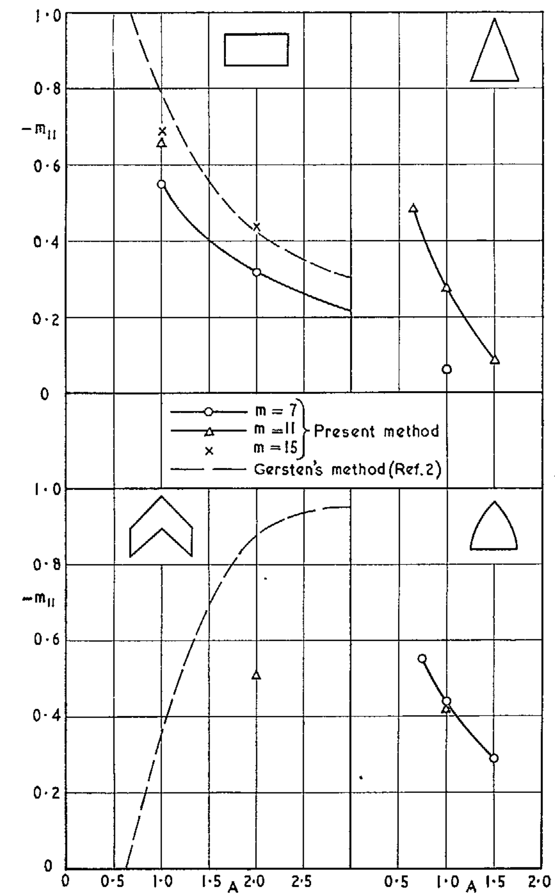

FIG. 4. Non-linear pitching-moment coefficient $(= m_{11}\alpha^2)$.

(89884)

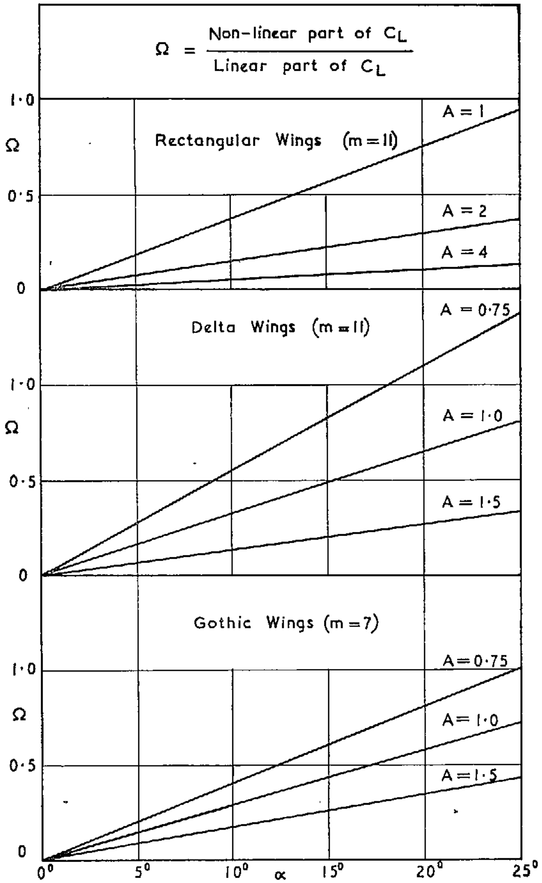

FIG. 5. Ratio of non-linear to linear theoretical lift.

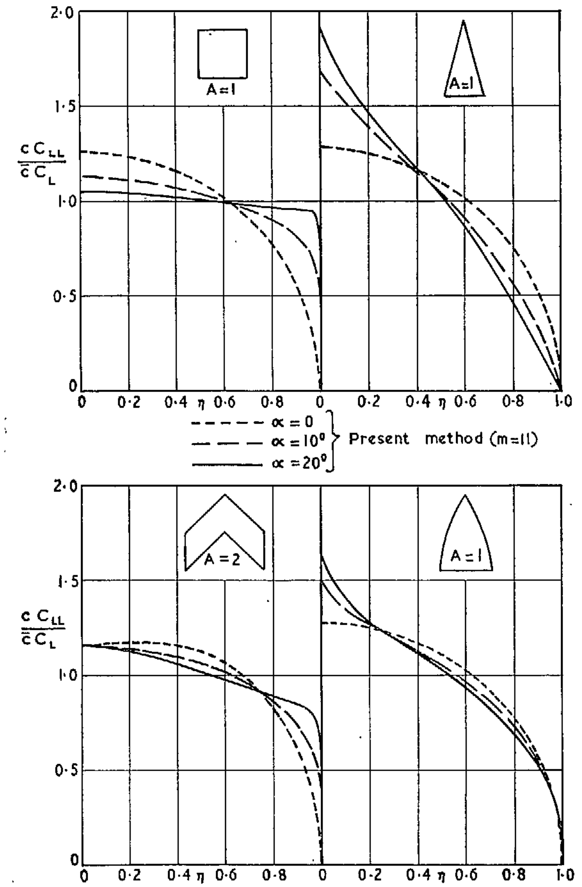

FIG. 6. Calculated spanwise loadings on various wings.

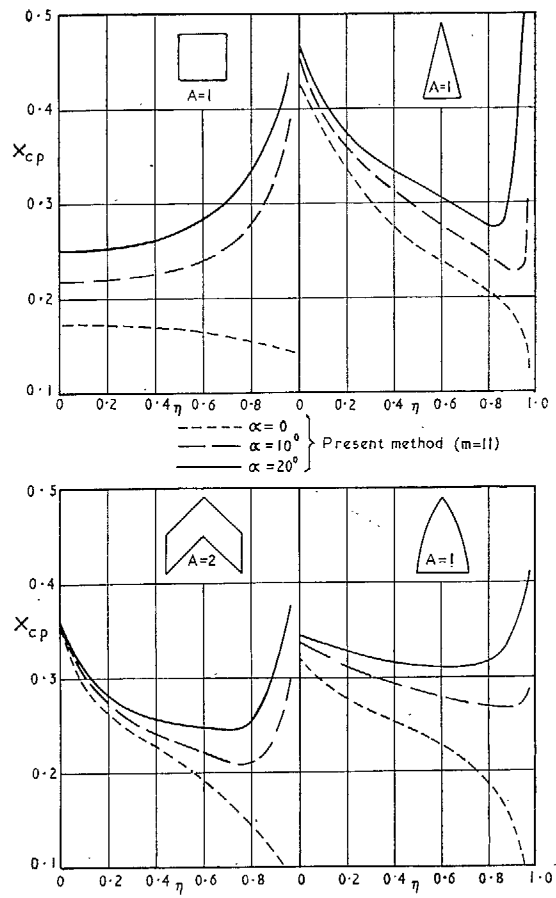

FIG. 7. Calculated spanwise distributions of centre of pressure.

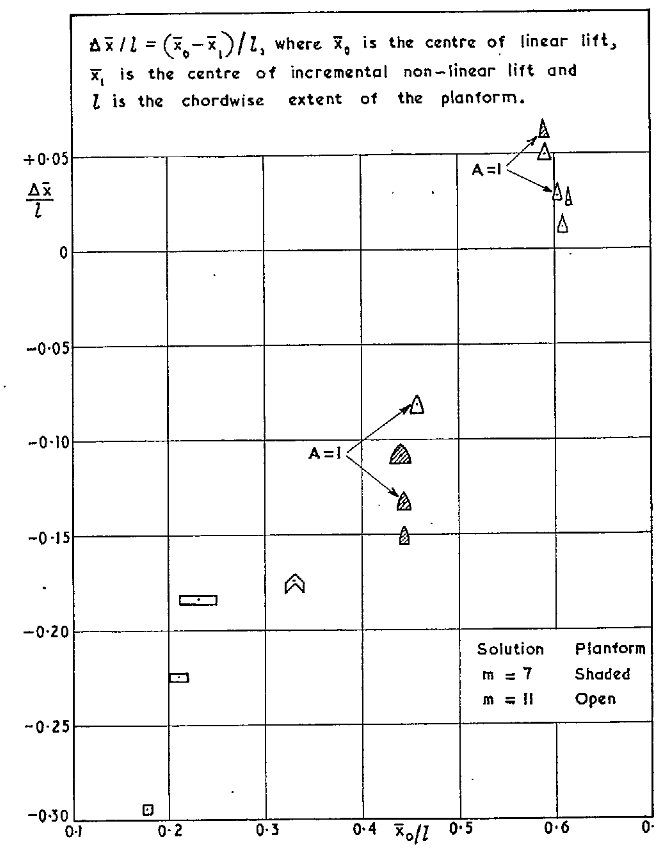

FIG. 8. Distance between centres of linear and non-linear theoretical lift for eleven planforms.

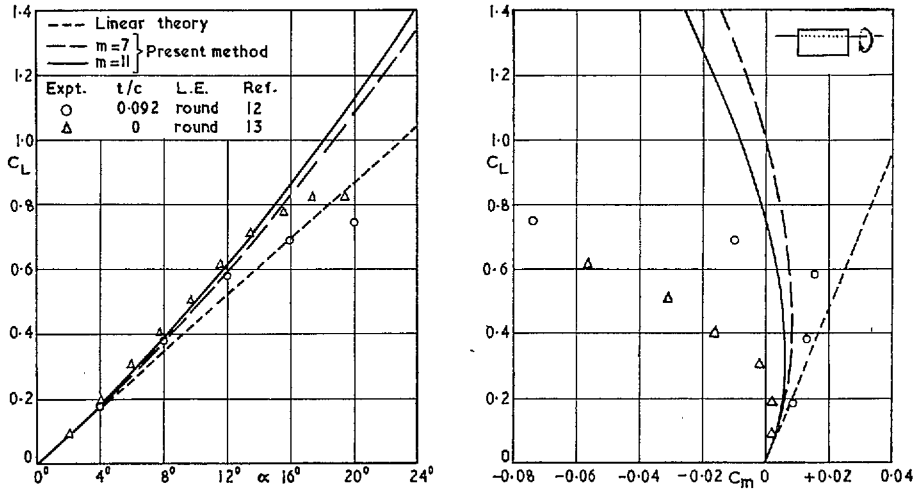

FIG. 9. Lift against incidence and pitching moment for a rectangular wing (A = 2).

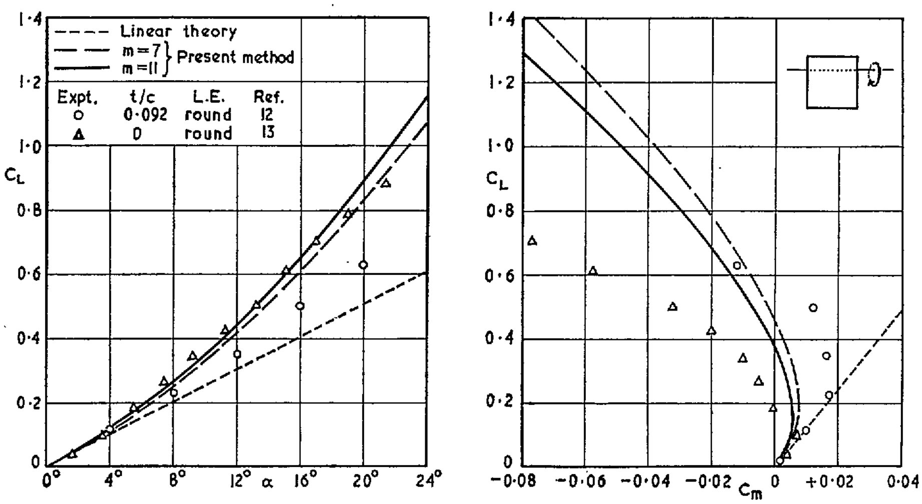

FIG. 10. Lift against incidence and pitching moment for a rectangular wing (A = 1).

(89884) E 2

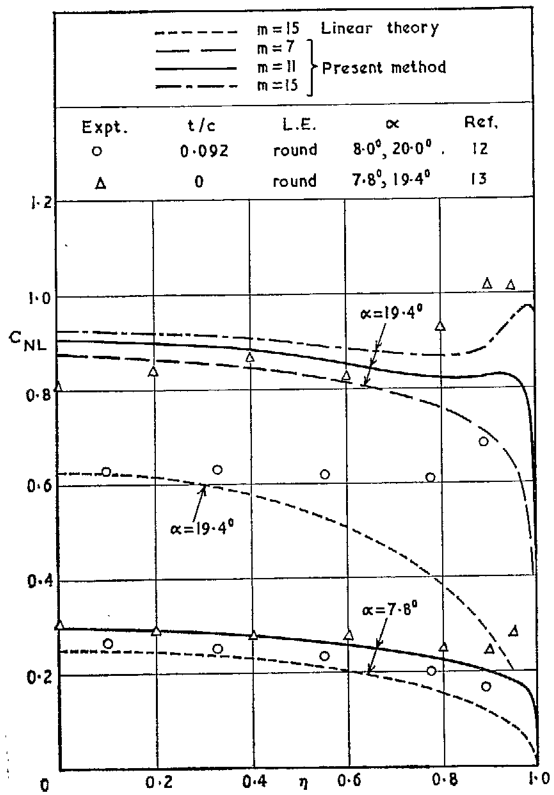

FIG. 11. Spanwise distributions of normal force for a rectangular wing ($A = 1$).

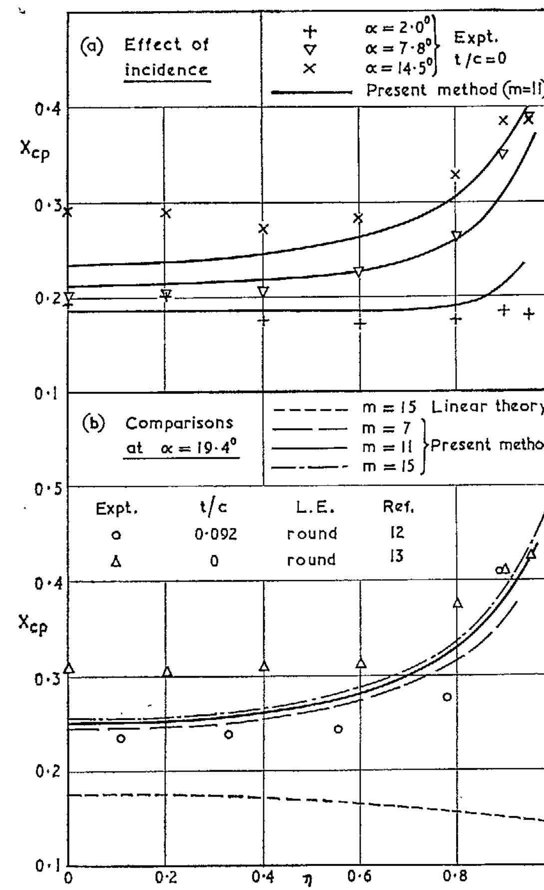

FIG. 12. Local centres of pressure for a rectangular wing ($A = 1$).

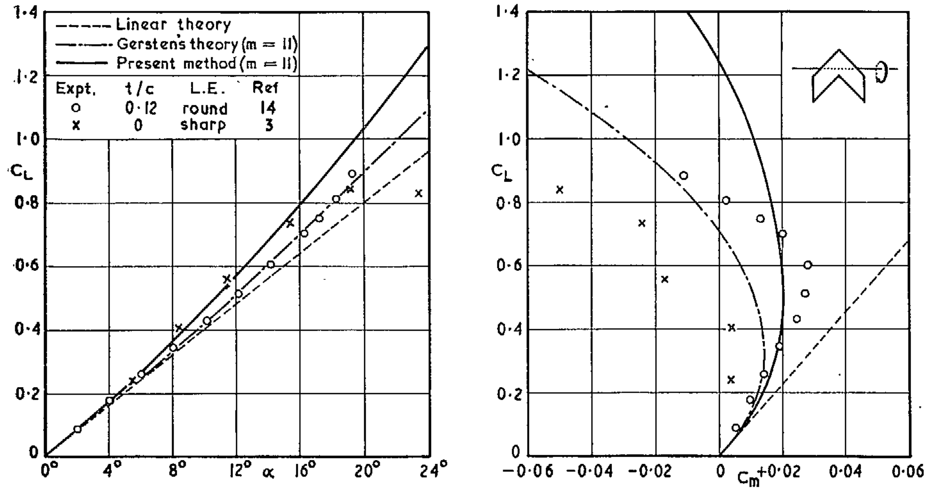

FIG. 13. Lift against incidence and pitching moment for a constant-chord wing ($\Lambda = 45°$, $A = 2$).

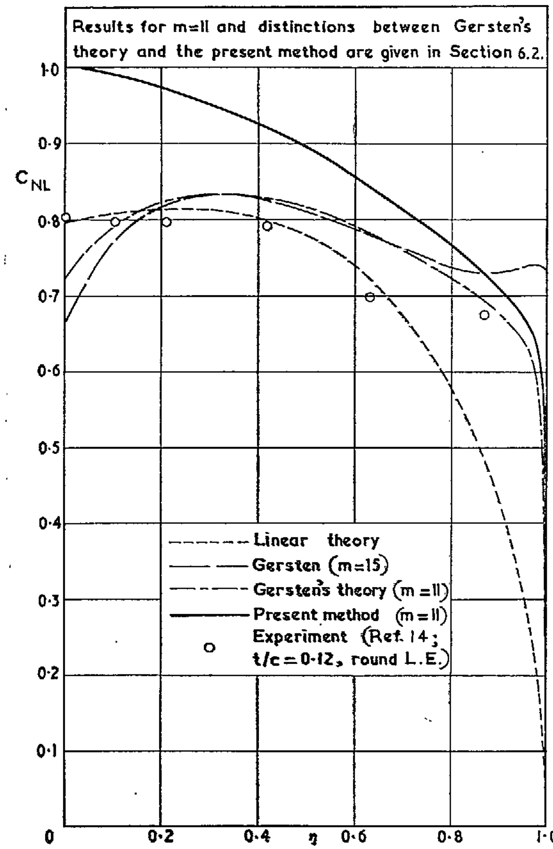

FIG. 14. Spanwise distributions of normal force for a constant-chord wing ($\Lambda = 45°$, $A = 2$) at $\alpha = 17 \cdot 3°$.

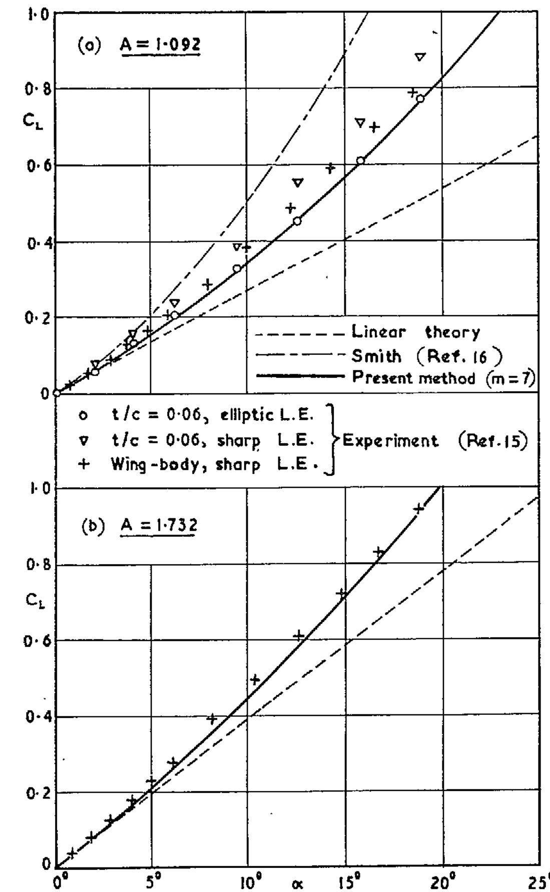

FIG. 15. Lift against incidence for two gothic wings.

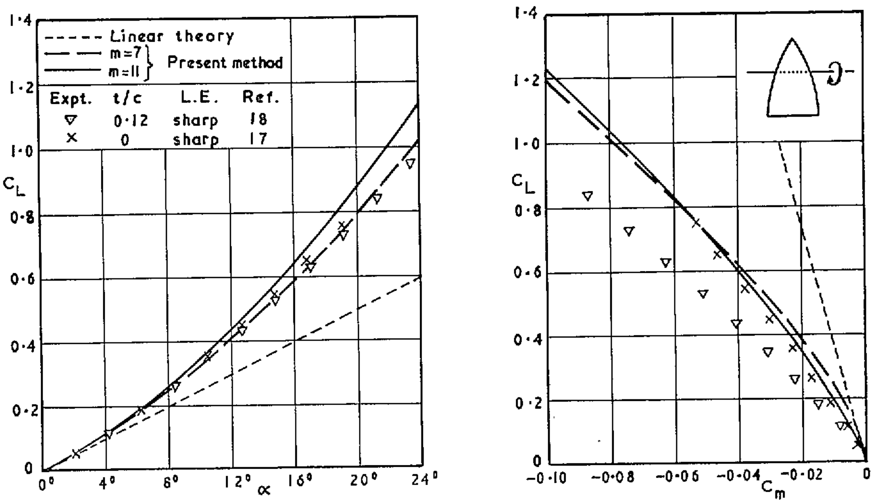

FIG. 16. Lift against incidence and pitching moment for a gothic wing ($A = 1$).

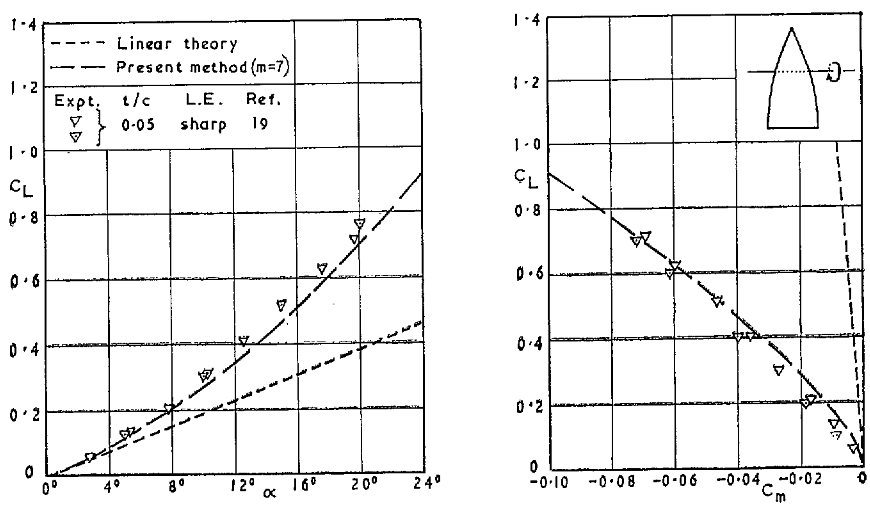

FIG. 17. Lift against incidence and pitching moment for a gothic wing ($A = 0{\cdot}75$).

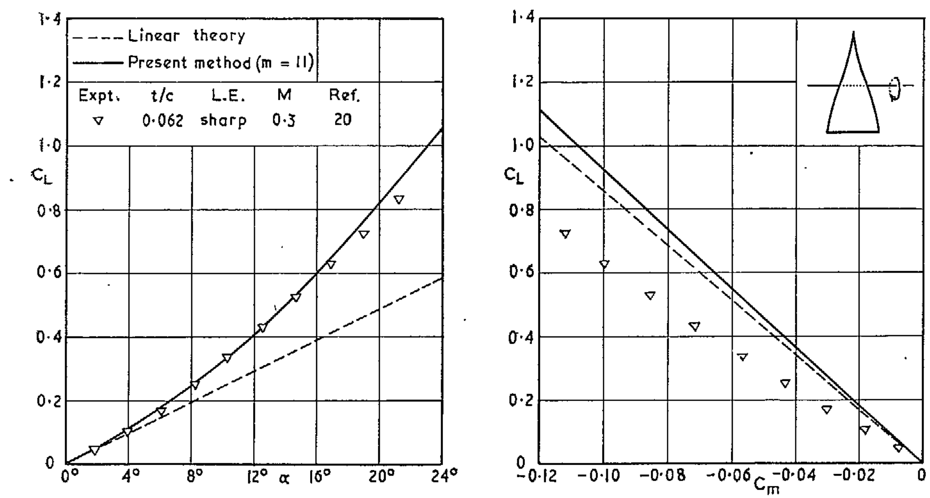

FIG. 18. Lift against incidence and pitching moment for an ogee wing ($A = 1$).

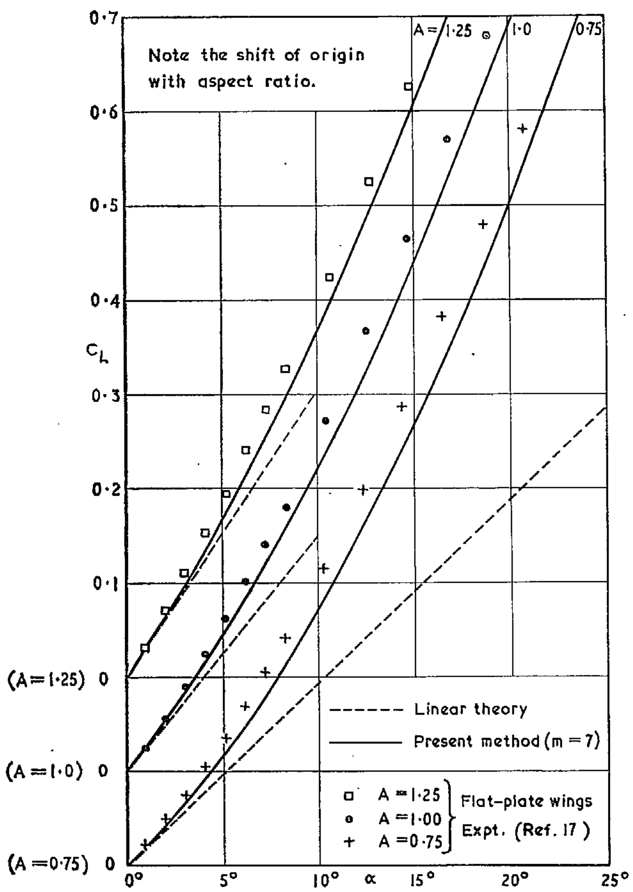

FIG. 19. Calculated and measured lift for three gothic wings.

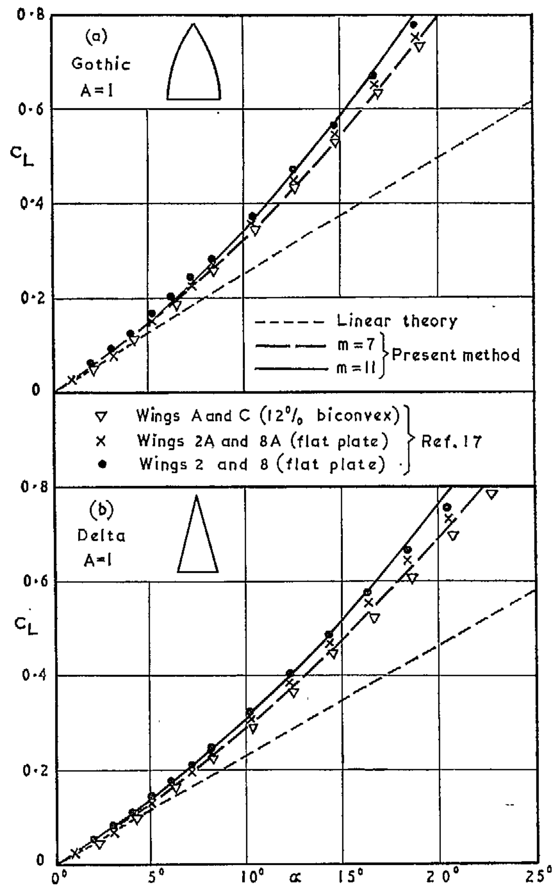

FIG. 20. Lift against incidence for wings of different section.

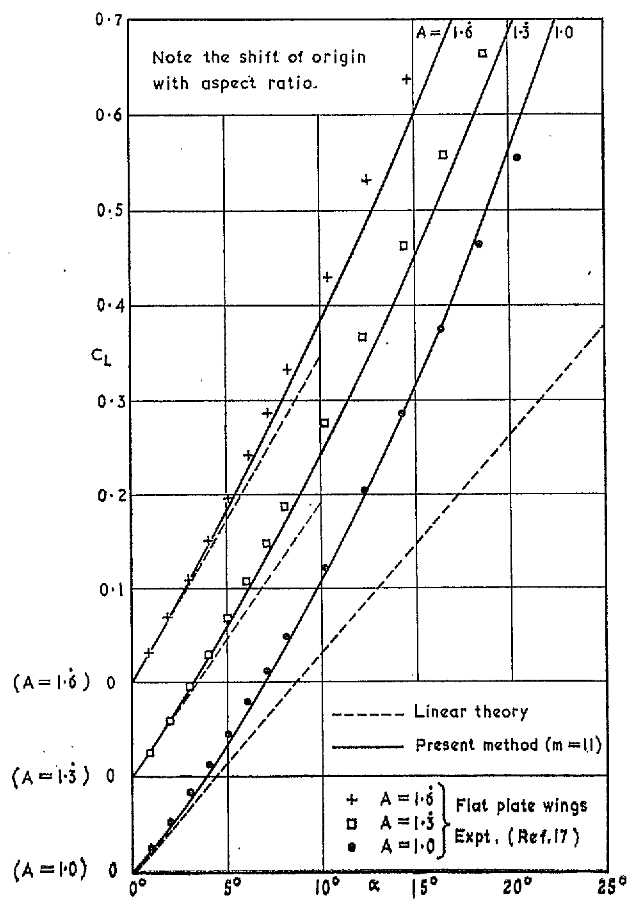

FIG. 21. Calculated and measured lift for three delta wings.

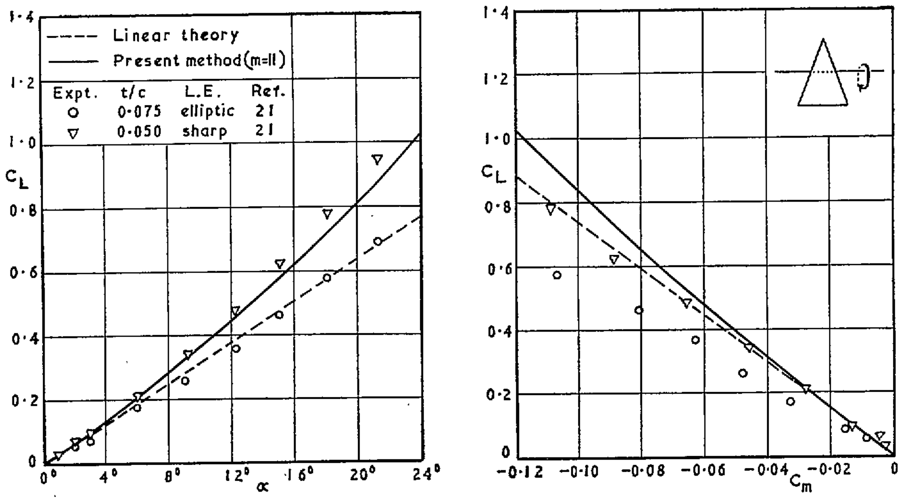

FIG. 22. Lift against incidence and pitching moment for a delta wing ($A = 1 \cdot 5$).

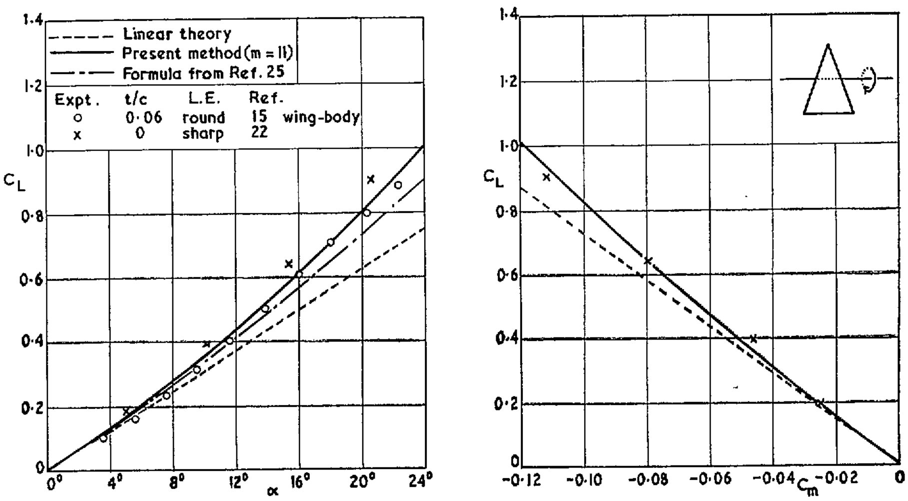

FIG. 23. Lift against incidence and pitching moment for a delta wing ($A = 1 \cdot 456$).

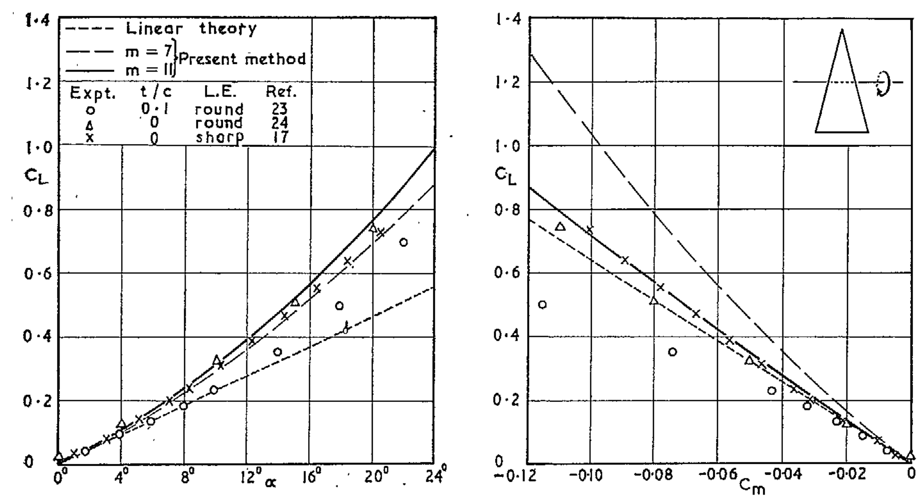

FIG. 24. Lift against incidence and pitching moment for a delta wing ($A = 1$).

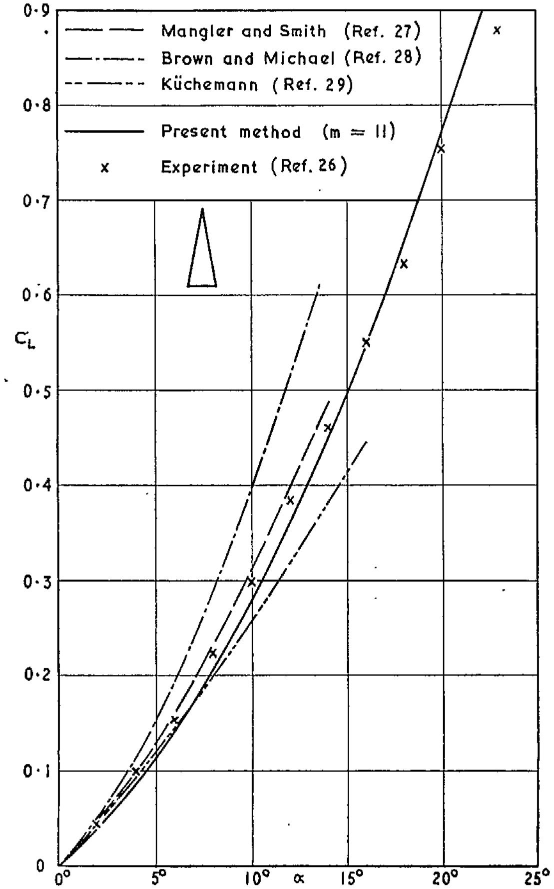

FIG. 25. Theoretical comparisons with measured lift on a delta wing ($A = 0{\cdot}7$).

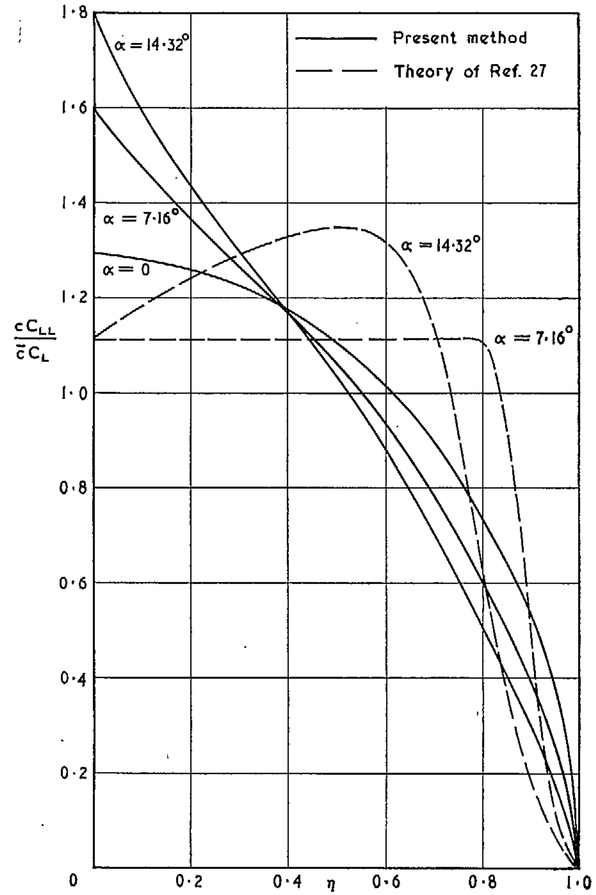

FIG. 26. Theoretical spanwise loadings for a delta wing ($A = 1$).

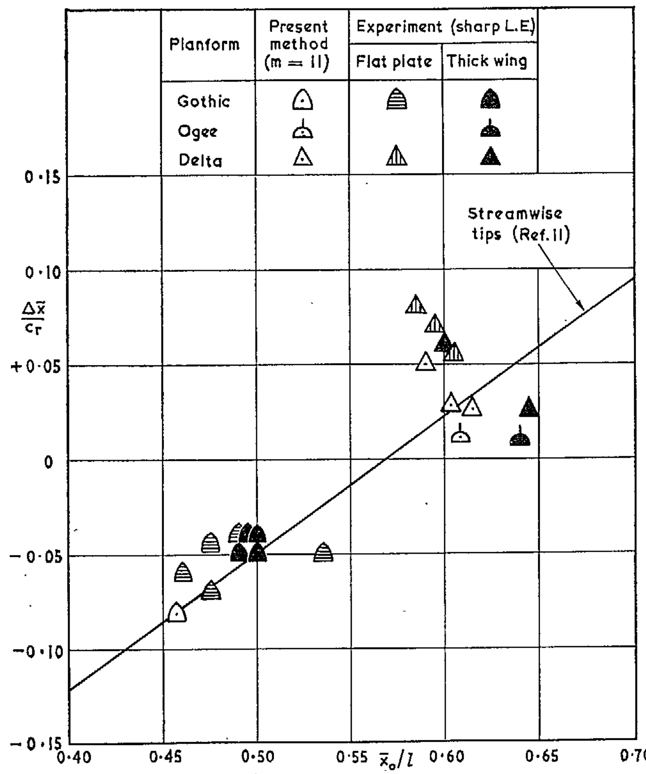

FIG. 27. Calculated and measured distance between centres of linear and non-linear lift.

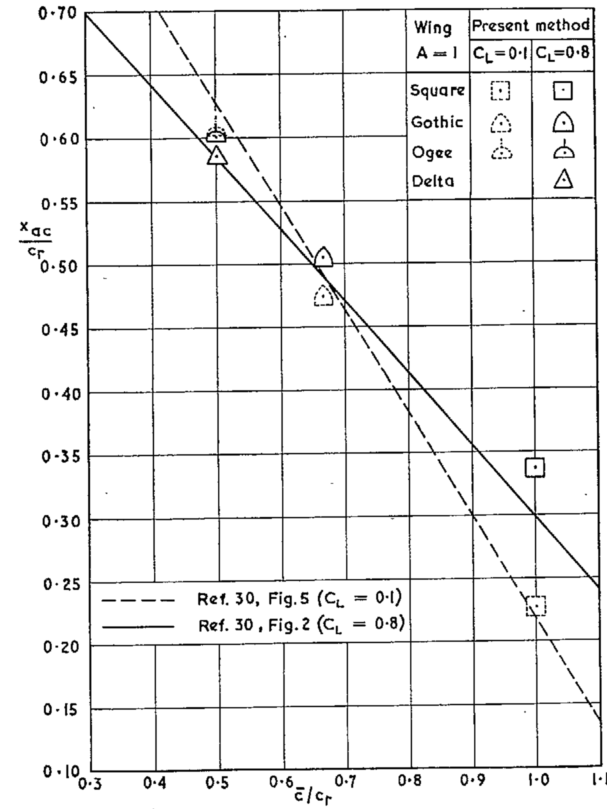

FIG. 28. Aerodynamic centre of wings (A = 1) at $C_L = 0·1$ and $0·8$.

(89884) Wt. 66/1418 K.5 8/64 Hw.

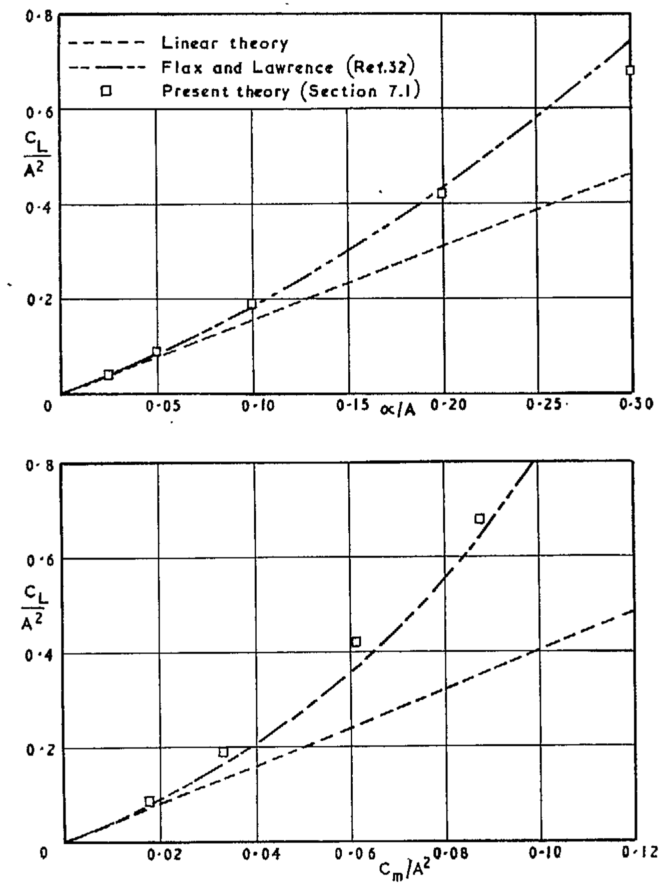

FIG. 29. Theoretical forces on slender rectangular wings.

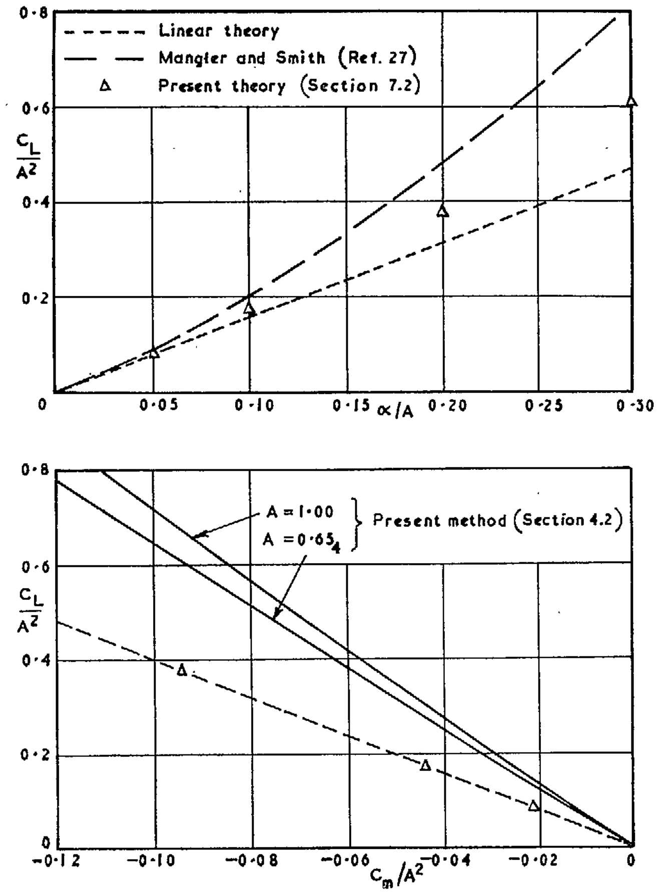

FIG. 30. Theoretical forces on slender delta wings.

Publications of the Aeronautical Research Council

ANNUAL TECHNICAL REPORTS OF THE AERONAUTICAL RESEARCH COUNCIL (BOUND VOLUMES)

1942 Vol. I. Aero and Hydrodynamics, Aerofoils, Airscrews, Engines. 75*s.* (post 2*s.* 9*d.*)
Vol. II. Noise, Parachutes, Stability and Control, Structures, Vibration, Wind Tunnels. 47*s.* 6*d.* (post 2*s.* 3*d.*)

1943 Vol. I. Aerodynamics, Aerofoils, Airscrews. 80*s.* (post 2*s.* 6*d.*)
Vol. II. Engines, Flutter, Materials, Parachutes, Performance, Stability and Control, Structures. 90*s.* (post 2*s.* 9*d.*)

1944 Vol. I. Aero and Hydrodynamics, Aerofoils, Aircraft, Airscrews, Controls. 84*s.* (post 3*s.*)
Vol. II. Flutter and Vibration, Materials, Miscellaneous, Navigation, Parachutes, Performance, Plates and Panels, Stability, Structures, Test Equipment, Wind Tunnels. 84*s.* (post 3*s.*)

1945 Vol. I. Aero and Hydrodynamics, Aerofoils. 130*s.* (post 3*s.* 6*d.*)
Vol. II. Aircraft, Airscrews, Controls. 130*s.* (post 3*s.* 6*d.*)
Vol. III. Flutter and Vibration, Instruments, Miscellaneous, Parachutes, Plates and Panels, Propulsion. 130*s.* (post 3*s.* 3*d.*)
Vol. IV. Stability, Structures, Wind Tunnels, Wind Tunnel Technique. 130*s.* (post 3*s.* 3*d.*)

1946 Vol. I. Accidents, Aerodynamics, Aerofoils and Hydrofoils. 168*s.* (post 3*s.* 9*d.*)
Vol. II. Airscrews, Cabin Cooling, Chemical Hazards, Controls, Flames, Flutter, Helicopters, Instruments and Instrumentation, Interference, Jets, Miscellaneous, Parachutes. 168*s.* (post 3*s.* 3*d.*)
Vol. III. Performance, Propulsion, Seaplanes, Stability, Structures, Wind Tunnels. 168*s.* (post 3*s.* 6*d.*)

1947 Vol. I. Aerodynamics, Aerofoils, Aircraft. 168*s.* (post 3*s.* 9*d.*)
Vol. II. Airscrews and Rotors, Controls, Flutter, Materials, Miscellaneous, Parachutes, Propulsion, Seaplanes, Stability, Structures, Take-off and Landing. 168*s.* (post 3*s.* 9*d.*)

1948 Vol. I. Aerodynamics, Aerofoils, Aircraft, Airscrews, Controls, Flutter and Vibration, Helicopters, Instruments, Propulsion, Seaplane, Stability, Structures, Wind Tunnels. 130*s.* (post 3*s.* 3*d.*)
Vol. II. Aerodynamics, Aerofoils, Aircraft, Airscrews, Controls, Flutter and Vibration, Helicopters, Instruments, Propulsion, Seaplane, Stability, Structures, Wind Tunnels. 110*s.* (post 3*s.* 3*d.*)

Special Volumes

Vol. I. Aero and Hydrodynamics, Aerofoils, Controls, Flutter, Kites, Parachutes, Performance, Propulsion, Stability. 126*s.* (post 3*s.*)
Vol. II. Aero and Hydrodynamics, Aerofoils, Airscrews, Controls, Flutter, Materials, Miscellaneous, Parachutes, Propulsion, Stability, Structures. 147*s.* (post 3*s.*)
Vol. III. Aero and Hydrodynamics, Aerofoils, Airscrews, Controls, Flutter, Kites, Miscellaneous, Parachutes, Propulsion, Seaplanes, Stability, Structures, Test Equipment. 189*s.* (post 3*s.* 9*d.*)

Reviews of the Aeronautical Research Council

1939–48 3*s.* (post 6*d.*) 1949–54 5*s.* (post 5*d.*)

Index to all Reports and Memoranda published in the Annual Technical Reports

1909–1947 R. & M. 2600 (out of print)

Indexes to the Reports and Memoranda of the Aeronautical Research Council

Between Nos. 2351–2449	R. & M. No. 2450	2*s.* (post 3*d.*)
Between Nos. 2451–2549	R. & M. No. 2550	2*s.* 6*d.* (post 3*d.*)
Between Nos. 2551–2649	R. & M. No. 2650	2*s.* 6*d.* (post 3*d.*)
Between Nos. 2651–2749	R. & M. No. 2750	2*s.* 6*d.* (post 3*d.*)
Between Nos. 2751–2849	R. & M. No. 2850	2*s.* 6*d.* (post 3*d.*)
Between Nos. 2851–2949	R. & M. No. 2950	3*s.* (post 3*d.*)
Between Nos. 2951–3049	R. & M. No. 3050	3*s.* 6*d.* (post 3*d.*)
Between Nos. 3051–3149	R. & M. No. 3150	3*s.* 6*d.* (post 3*d.*)

HER MAJESTY'S STATIONERY OFFICE

from the addresses overleaf

Printed and published by
HER MAJESTY'S STATIONERY OFFICE

To be purchased from
York House, Kingsway, London W.C.2
423 Oxford Street, London W.1
13A Castle Street, Edinburgh 2
109 St. Mary Street, Cardiff
39 King Street, Manchester 2
50 Fairfax Street, Bristol 1
35 Smallbrook, Ringway, Birmingham 5
80 Chichester Street, Belfast 1
or through any bookseller

Printed in England

R. & M. No. 3375

S.O. Code No. 23-3375